

**DEVELOPMENT OF PEG AND PEG-PEPTIDE
BASED DRUG DELIVERY SYSTEMS**

**A Thesis Submitted to
the Graduate School of Engineering and Sciences of
İzmir Institute of Technology
in Partial Fulfillment of the Requirements for the Degree of
MASTER OF SCIENCE
in Chemical Engineering**

**by
Beste BALCI**

June 2016

İZMİR

We approve the thesis of **Beste BALCI**

Examining Committee Members:

Assist. Prof. Dr. Ayben TOP

Department of Chemical Engineering, Izmir Institute of Technology

Prof. Dr. Sacide ALSOY ALTINKAYA

Department of Chemical Engineering, Izmir Institute of Technology

Prof. Dr. Hatice Yeşim KARASULU

Department of Pharmaceutical Technology, Ege University

27 July 2016

Assist. Prof. Dr. Ayben TOP

Supervisor, Department of Chemical Engineering
Izmir Institute of Technology

Prof. Dr. Fehime Seher ÖZKAN

ÇAKICIOĞLU

Head of the Department of Chemical
Engineering

Prof. Dr. Bilge KARAÇALI

Dean of the Graduate School
of Engineering and Sciences

ACKNOWLEDGMENTS

I heartily would like to express my gratitude to my advisor, Assist. Prof. Dr. Ayben TOP whose knowledge, encouragement and valuable suggestions have broadened my mind and helped me to complete M.Sc. studies. I am also thankful to my committee members, Prof. Dr. Sacide ALSOY ALTINKAYA and Prof. Dr. Hatice Yeşim KARASULU for serving as my committee members and sparing their valuable time during my thesis defense seminar.

I indebted to Prof. Dr. Talat YALÇIN and Dr. Ahmet Emin ATİK for kindly providing mass spectroscopy data, which were taken at Biological Mass Spectrometry and Proteomics Facility at Izmir Institute of Technology. I really appreciate Research Assistant Fırat ZIYANAK for taking NMR data. I would like to express my appreciation to Prof. Dr. Mehmet POLAT and Prof. Dr. Muhsin ÇİFTÇİOĞLU for making the equipment in their laboratory easily accessible for me. In addition, I am grateful to Technical Stuff Belgin TUNÇEL KIRKAR, Specialist Deniz ŞİMŞEK, Dr. Burcu ALP and Dr. Gülnihal ÖZEK YELKEN in Chemical Engineering Department along with Specialist Özgür YILMAZER, Specialist Yekta GÜNAY OĞUZ, Specialist Dane RUSÇUKLU and Specialist Evrim BALCI in BİYOMER for their help in all of my characterization studies. I wish to thank the whole staff in Department of Chemical Engineering for their help and technical assistance.

I would also like to thank TÜBİTAK for financial support (3501 Career Project # 112S554, PI = Assist. Prof. Ayben Top) and facilitating me to work in this valuable project.

My friends' help can not be underestimated in this thesis. I would like to thank especially to Nesligül YÜKSEL for her friendship and co-work in the laboratory.

All my studies would not have been possible without the support of my family. I would like to express my gratitude to my parents and sister for their understanding and support throughout my life. They have encouraged me all the time in my M.Sc.

ABSTRACT

DEVELOPMENT OF PEG AND PEG-PEPTIDE BASED DRUG DELIVERY SYSTEMS

In this study, two types of drug delivery systems (DDS) were prepared; mPEG (methoxy polyethylene glycol)-HYD (hydrazide)-DOX and mPEG-peptide-(HYD)-DOX. In the design of the conjugates, mPEG was used to increase the blood circulation time. HYD provided an acid cleavable bond between the carrier molecule and DOX, whereas peptide containing histidines imparted pH responsiveness of the molecule. Doxorubicin (DOX) was selected as a model anti-cancer drug. DDS were synthesized using two steps; hydrazide functionalization of carboxylic acid of the carrier molecule followed by DOX conjugation. Hydrazide form of the carrier molecules denoted as HYD1 and HYD2 were obtained using adipic acid dihydrazide (AADH) and carbohydrazide (CH), respectively. To increase DOX conjugation, trifluoroacetic acid (TFA) and DOX amounts were changed and the reactions were carried out at the conditions giving the highest DOX conjugation (mPEG-HYD:DOX:TFA= 2.5mg:2mg:20 μ L per 1 mL of DMSO). The peptide (AT1=CGGGHHHHHHGGGE) was synthesized using solid phase peptide synthesis (SPPS) and PEGylated using mPEG-maleimide to obtain mPEG-AT1 conjugate. The purity of AT1 and mPEG-AT1 were confirmed using mass spectroscopy and high performance liquid chromatography (HPLC). DOX conjugation percentages were obtained as 62 ± 7 , 60 ± 3 and 35 ± 3 for mPEG-HYD1-DOX, mPEG-HYD2-DOX and mPEG-AT1-HYD1-DOX, respectively. Drug release studies indicated modest pH responsiveness of the carrier molecules obtained using AADH. On the other hand, mPEG-HYD2-DOX released $\sim 13\%$ of drug at the end of the 72h independent of pH. For mPEG-AT1-DOX, drug release percentage values were obtained as $\sim 15\%$ and $\sim 30\%$ at pH 7.4 and 5.0 respectively. Cytotoxicity of the conjugates of DDS was determined using lung cancer (A-549) cell lines. DOX equivalent IC₅₀ values were determined as 20, 40 and 5 for mPEG-HYD1-DOX, mPEG-HYD2-DOX and mPEG-AT1-DOX respectively.

ÖZET

PEG VE PEG-PEPTİT BAZLI İLAÇ TAŞIYICI SİSTEMLERİNİN GELİŞTİRİLMESİ

Bu çalışmada, iki çeşit ilaç taşıyıcı sistemi hazırlanmıştır; mPEG (metoksi polietilen glikol)-HYD (hidrazit)-DOX ve mPEG-peptit-(HYD)-DOX. Konjugatların tasarımında kanda dolaşım süresini artırmak için PEG kullanılmıştır. HYD, taşıyıcı molekül ve DOX arasında asit bozunur bağ olma özelliğini sağlarken histidin içeren peptit, moleküle pH cevaplayabilen bir özellik sağlamıştır. Model bir kanser ilacı olarak DOX seçilmiştir. İlaç taşıyıcı sistemi taşıyıcı molekülün karboksilik asitinin hidrazit modifikasyonunun gerçekleştirilmesi ve ardından DOX konjugasyonu olmak üzere iki aşamada sentezlenmiştir. Adipik asit dihidrazit (AADH) ve karbohidrazit (CH) kullanılarak HYD1 ve HYD2 olarak tanımlanan taşıyıcı moleküllerin hidrazit formları sentezlenmiştir. DOX konjugasyon yüzdesini artırmak için TFA ve DOX miktarları değiştirilmiş ve reaksiyonlar en yüksek DOX konjugasyonunu verecek şekilde gerçekleştirilmiştir (mPEG-HYD:DOX:TFA = 2.5mg:2mg:20µL / 1 ml DMSO). Katı faz peptit sentezi ile AT1 = CGGGHHHHHHGGGE peptiti sentezlenmiş ve mPEG-maleimit ile konjugasyonu yapılması sonucu mPEG-AT1 elde edilmiştir. AT1 ve mPEG-AT1'in saflığı kütle spektroskopisi ve HPLC ile belirlenmiştir. mPEG-HYD1-DOX, mPEG-HYD2-DOX ve mPEG-AT1-DOX'un konjugasyon yüzdeleri sırasıyla 62 ± 7 , 60 ± 3 ve 35 ± 3 olarak elde edilmiştir. İlaç salım çalışmalarında AADH'nin kullanıldığı taşıyıcı moleküllerde makul bir pH cevaplayabilir özelliği elde edilmiştir. Diğer taraftan, pH'tan bağımsız olarak 72 saat sonunda mPEG-HYD2-DOX, ilacın \sim % 13'ünü salmıştır. mPEG-AT1-DOX için ilaç salım yüzdeleri pH 7.4 ve pH 5.0 için sırasıyla \sim % 15 ve \sim % 30 olarak elde edilmiştir. Konjugatların sitotoksitesi, akciğer kanseri hücre (A-549) hattı kullanılarak gerçekleştirilmiştir. DOX eşdeğer IC_{50} değerleri, mPEG-HYD1-DOX, mPEG-HYD2-DOX ve mPEG-AT1-HYD1-DOX için sırasıyla 20, 40 ve 5 µg/ml olarak belirlenmiştir.

TABLE OF CONTENTS

LIST OF FIGURES.....	viii
LIST OF TABLES.....	x
CHAPTER 1. INTRODUCTION.....	1
CHAPTER 2. LITERATURE REVIEW.....	5
2.1. Progression of Cancer Cells and Treatment Methods.....	5
2.2. Cancer Cell Properties and Ideal Drug Delivery Systems.....	9
2.2.1. DDS Based on Physical Interactions Between the Drug and Carrier.....	12
2.2.2. Drug Conjugated Delivery Systems.....	14
CHAPTER 3. MATERIALS AND METHODS.....	17
3.1. Materials.....	17
3.2. Methods.....	18
3.2.1. Preparation of Methoxy Polyethylene Glycol-Hydrazone- Doxorubicin (mPEG-HYD-DOX) Conjugates.....	18
3.2.1.1. mPEG – HYD Synthesis.....	18
3.2.1.2. Doxorubicin (DOX) Conjugation to mPEG-HYD.....	20
3.2.2. Preparation of mPEG-Peptide-HYD-DOX Conjugate.....	22
3.2.2.1. Peptide Synthesis.....	23
3.2.2.2. mPEG-Peptide Synthesis.....	23
3.2.2.3. mPEG-Peptide-DOX Conjugate Synthesis.....	25
3.3. Characterization.....	26
3.3.1. NMR Analysis.....	26
3.3.2. Fourier Transform Infrared Spectroscopy (FTIR) Analysis.....	27
3.3.3. High Performance Liquid Chromotography (HPLC).....	28
3.3.4. Mass Spectroscopy.....	28
3.3.5. UV Vis Spectroscopy.....	29

3.3.6. Determination of Aggregation State.....	29
3.3.7. Drug Release.....	30
3.3.8. Cytotoxicity Test.....	30
CHAPTER 4. RESULTS AND DISCUSSIONS.....	33
4.1. Preparation of PEG based DDS	33
4.2. Preparation of PEG-Peptide based DDS	38
4.2.1. Peptide (AT1) Synthesis.....	38
4.2.2. PEG-Peptide Conjugation	39
4.3. DOX Conjugation to PEG and PEG-peptide based DDS.....	41
4.4. Characterization of DOX Conjugated Drug Delivery Systems.....	43
4.4.1. Size Measurement.....	43
4.4.2. Drug Release Profiles.....	47
4.4.3. Cytotoxicity.....	50
CHAPTER 5. CONCLUSIONS.....	53
REFERENCES.....	54
APPENDIX A. SUPPLEMENTARY FIGURES AND CALCULATIONS.....	64

LIST OF FIGURES

<u>Figure</u>	<u>Page</u>
Figure 1.1. Examples of Different Forms of Drug Delivery Systems.....	2
Figure 2.1. Evolution of Cancer from Environmental Risk Factors.....	7
Figure 2.2. Human Lymphoma Exposed to Camptothecin.....	9
Figure 2.3. Illustration of EPR Effect.....	10
Figure 2.4. pH Programmed Drug Release at Cellular Compartments.....	11
Figure 2.5. Comparison of the Cytotoxicity of Paclitaxel Loaded PCL and PbAE Nanoparticles.....	12
Figure 2.6. Paclitaxel Release of Poly(PbAE-g-PEG) at pH 5.0 and 7.4.....	13
Figure 2.7. pH Programmed Release of Pyrene from poly(HF-b-PEG).....	14
Figure 2.8. DOX Release Curves of PEG-g-DOX at Different pH Values	15
Figure 2.9. Endosomal Cleavage of Hydrazone Bond of a Prodrug	15
Figure 2.10. Synthesis of PEG-p(Asp-Hyd-ADR) Block Copolymers.....	16
Figure 2.11. DOX Release from the PEG-p(Asp-Hyd-ADR) Block Copolymer.....	16
Figure 3.1. Reaction Scheme of mPEG-HYD1.....	19
Figure 3.2. Reaction Scheme of mPEG-HYD2.....	19
Figure 3.3. Conjugation Reaction of DOX to mPEG-HYD1.....	21
Figure 3.4. Conjugation reaction of DOX to mPEG-HYD2.....	22
Figure 3.5. Reaction Scheme of mPEG-AT1.....	24
Figure 3.6. Synthesis of mPEG-AT1-HYD1.....	25
Figure 3.7. Reaction Scheme of mPEG-AT1-DOX	27
Figure 3.8. Conversion of Tetrazolium Salt to Formazan Crystals.....	31
Figure 4.1. FTIR Spectra of mPEG-propionic acid, mPEG-HYD1 and mPEG-HYD2.....	35
Figure 4.2. NMR Spectrum of mPEG-COOH in D ₂ O	36
Figure 4.3. NMR Spectrum of mPEG-HYD1 in D ₂ O.....	36
Figure 4.4. NMR Spectrum of mPEG-HYD1 (Twice Reaction with AADH) in D ₂ O.....	37
Figure 4.5. ESI-MS Spectrum of AT1 Peptide	38

Figure 4.6.	HPLC Curves of AT1, mPEG-MAL, and mPEG-AT1	39
Figure 4.7.	MALDI-TOF Spectrum of mPEG-AT1	40
Figure 4.8.	FTIR Spectra of (a) AT1, (b) mPEG-MAL, and (c) mPEG-AT1	41
Figure 4.9.	Size Distribution of PEGs with Different Functional Groups and PEG-AT1 Conjugate	44
Figure 4.10.	Size Distributions of the As prepared DOX-Conjugated DDS	45
Figure 4.11.	Size Distributions of the DOX-Conjugated DDS Obtained After 24 hrs Incubation	46
Figure 4.12.	mPEG-HYD1-DOX Drug Release Curves at pH 5.0 and 7.4	49
Figure 4.13.	mPEG-HYD2-DOX Drug Release Curves at pH 5.0 and 7.4	49
Figure 4.14.	mPEG-AT1-DOX Drug Curves Release at pH 5.0 and 7.4	50
Figure 4.15.	Cytotoxicity of mPEG-COOH, AADH, mPEG-HYD1, and AT1	51
Figure 4.16.	Growth Inhibition Curves of Free DOX and DOX-Conjugated DDS	52

LIST OF TABLES

<u>Table</u>		<u>Page</u>
Table 2.1.	Examples of Genetic Changes in Cells.....	6
Table 3.1.	DOX Conjugation Experiments.....	21
Table 4.1.	Optimization of DOX Functionalization.....	42
Table 4.2.	PEG and PEG-Peptide based DDS used for DOX Conjugation.....	42
Table 4.3.	DOX Conjugation Yields and % of the DDS.....	43
Table 4.4.	Comparison of Drug Release % Values of Various DDS at Neutral and Acidic pH.....	50
Table 4.5.	IC ₅₀ Values of the Samples.....	52

CHAPTER 1

INTRODUCTION

Development of drug delivery systems (DDS) has gained great importance in the recent years as the introduction of a new drug into the market is costly and a time consuming process. (Tiwari et al., 2012). To extend patented life of a drug, patents of controlled release formulations of the same drug have been developed. Thus, instead of discovering new drugs, much of the efforts have been spent on improving some properties of DDS. An ideal drug delivery system should be designed to carry sufficient drug to the target site without leakage during the transit by facilitating the recovery of disease at effective dose with minimal toxic effect (Florence et al., 1993; Tong et al., 2007).

Drug delivery systems can be designed in different structures such as polymer-drug conjugates, micelles, nanospheres, nanogels, vesicles and dendrimers (Farokhzad et al., 2006). Examples of drug carriers and their characteristic sizes are shown in Figure 1.1 (Tong et al., 2007). Of these structures, nanocarriers in the form of polymeric micelles containing drugs conjugated or encapsulated have been proposed in cancer therapy as a targeting strategy to exploit enhanced permeation and retention (EPR) effect observed in cancer cells.

Micelles are formed when amphiphilic molecules (containing both hydrophilic and hydrophobic groups) self-assemble in aqueous solution to form core-shell structures above a certain concentration called critical micelle concentration (CMC). The inner core of micelle is condensed and can easily capture hydrophobic compounds like anticancer drugs. Since polymeric micelles in the range of 20-100 nm are more resistant and stable than other types of micelles, they have become a usual choice for drug delivery applications (Haag et al., 2004; Torchilin et al., 2005). It was confirmed that nanosized micelles could reach the pathological sites such as capillaries at sites of infection, inflammation solid tumors. Another advantage of small sized polymeric micelles is the ease of filtration for sterilization purposes requiring no further aseptic

sterilization processes. Additionally, superior to larger micelles, these nanosized micelles do not cause embolism of capillaries during the circulation (Kwon et al., 1996).

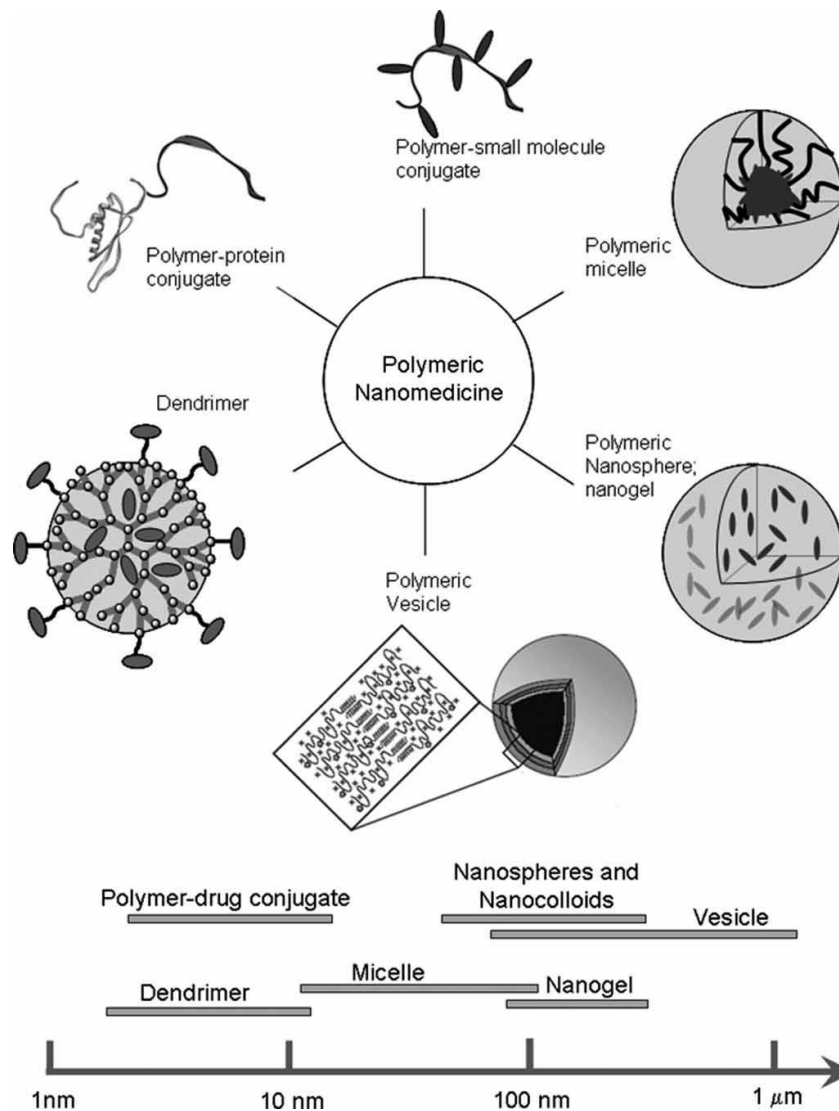


Figure 1.1. Examples of Different Forms of Drug Delivery Systems (Source: Tong et al., 2007).

Polymer-drug conjugates, in which drug is covalently attached to the carrier molecule, are another alternative drug delivery systems widely employed. Especially, hydrophilic polymers have been conjugated to the broad range therapeutics such as small molecular weight drugs, peptides, and antibodies to increase water solubility and to decrease immunogenicity effects. Another advantage of these polymeric therapeutic systems includes protection of drug from degradation or deactivation by increasing bioavailability and blood circulation time of the drug (Mero et al., 2009).

Dextran and poly(ethylene glycol) (PEG) are the two pioneer polymers used for drug conjugation (Wieder et al., 1979). PEG is water-soluble, biocompatible non-degradable and nontoxic polyether (<12 kDa). Unlike dextran, it is non-immunogenic (Veronese et al., 2002). In many studies, it was well documented that, PEGylation of drugs resulted in enhancement of therapeutic activity and blood circulation time of drug and reduction in immunogenicity (Chaffee et al., 1992; Cheng et al., 1997; Harris et al., 2003; Cheng et al., 2012). In addition to PEG-drug conjugates, PEGylated peptides and proteins have also been developed. One commercialized example of these systems is Oncaspar® (PEG-asparaginase) used in cancer therapy (Keating et al., 1993). Other widely used hydrophilic polymers include poly(N-(2-hydroxypropyl) methacrylamide) (HPMA) and poly(ethylene oxide) (PEO), which is a high molecular weight polyether.

Both micellar and conjugate systems can be designed to respond external stimuli such as pH, temperature, ionic strength and analyte concentration. For cancer therapy, pH responsive DDS have been proposed as they ensure fast release in endosomal components to overcome multidrug resistance. In DDS design, carrier molecule can have inherently pH responsive functional groups as in poly- β -amino-ester (PBAE) (Lee et al. 2003; Shen et al., 2009) or drug can be attached to the carrier molecule via pH responsive chemical bond such as hydrazone, acetal and ketal linkers (Bae et al., 2005; Gillies et al., 2005; Zhou et al., 2011). Drug delivery systems containing pH functional groups provide fast drug release at endosomal pH values. However, considerable leakage of drug also occurs at neutral pH resulted in side effects of the drug. On the other hand, covalent attachment of drug minimizes the release at neural pH but if the drug delivery system form micelles, slow release of the drug at acidic pH is also inevitable.

In this study, it was aimed to prepare and characterize pH responsive DDS containing both pH responsive functional groups and acid cleavable chemical bond to exploit the advantages of these drug delivery system configurations. The drug conjugate systems were obtained by covalently attaching doxorubicin (DOX) to the carrier molecules, PEG and PEG-peptide based systems. In these DDS, PEG was used as a hydrophilic block to increase solubility and increase blood circulation time of DDS during the transport. DOX was used as a model anticancer drug. DOX was attached to carrier molecules via acid cleavable hydrazone bond. Additionally, the designed peptide containing histidines were used to impart pH responsiveness to the carrier molecule. The experimental techniques employed to the synthesise DDS and the characterization

methods used are explained in Chapter 3. Chapter 4 includes the results of characterization methods used to assess purity of the carrier molecules along with the size distribution, drug release and cytotoxicity properties of the DOX-conjugated DDS proposed.

CHAPTER 2

LITERATURE REVIEW

2.1. Progression of Cancer Cells and Treatment Methods

Cancer, associated with toxicological substances, is the second fatal disease after cardiovascular disease. It is a broad term that covers variety of diseases. However, the common feature of all cancer types is the continuous cell proliferation that cannot be controlled by the normal cell kinetic regulators. Eventually, this abnormal growth of the cells is resulted in the development of solid tumors (lumps).

Carcinogenesis (tumor production) is a multi-step process with three main phases: initiation, promotion and progression (Berenblum et al., 1947). In the first step, initiation of carcinogenesis, the cellular genome undergoes mutations creating the potential for neoplastic (tumor) development (UNSCEAR, 1993; Cox et al., 1994). Basically, this step involves stable cellular changes induced by exposure to carcinogen. A notable example is a single point mutation that converts the Ha-ras proto-oncogene into a dominant oncogene (activated gene having the potential to cancer) (Tabin et al., 1982). The effects of such tumor gene mutations include cellular response, dysregulation of genes (i.e. biochemical signaling pathways related to control of cell proliferation, disruption of common cellular communication and development). Examples of genetic changes in cells are given in Table 2.1 (Barrett, 1993).

In the evolution of cancers, tumor-suppressor genes exist along with proto-oncogenes. When proto-oncogenes are activated by mutational mechanisms, positive proliferation of tumors appears. On the other hand, suppressor genes block the neoplastic growth of genes and inactivate tumor cells (Boyd et al., 1990). If the function of tumor suppressor gene is reduced, the cell is susceptible to cancer.

Promotion is the second step of carcinogenesis that follows initiation. The previously transformed (initiated) cell may remain harmless. However, further changes of an initiated cell with prolonged exposures lead to promotion step (Upton et al., 1986).

Progression is the third stage in which neoplasm gives rise increasingly to malignant sub-populations. Likewise in promotion step, the process may be accelerated by the repeated exposure to carcinogenic stimuli. In the first phase of progression (neoplastic conversion), pre-neoplastic cells are transformed to malignant ones (UNSCEAR, 2000).

Table 1.1. Examples of Genetic Changes in Cells
(Source: Barrett, 1993).

Type of genetic change	Examples
Gene mutation	Point mutation (G→T) in codon 12 of the <i>c-Ha-ras</i> gene in EJ/T24 bladder carcinoma Point mutation (A→G) in the splice acceptor sequence of exon 21 in the retinoblastoma gene of J82 bladder carcinoma cells
Chromosome rearrangement	Philadelphia translocation t(9;22) in chronic myelogenous leukemia, t(8;14) in Burkitt's lymphoma
Gene amplification	<i>N-myc</i> gene in neuroblastomas, <i>c-myc</i> gene in lung carcinomas, <i>neu</i> gene in mammary carcinomas
Aneuploidy	+12 in chronic lymphocytic leukemia, +8 in acute nonlymphocytic leukemia, blast phase of chronic myelogenous leukemia, +15 in murine T-cell leukemias, -22 in meningiomas, -15 in Syrian hamster tumors induced by transfection of <i>v-Ha-ras</i> and <i>v-myc</i>

Malignant development is related to the dynamic cellular heterogeneity leading to the acquisition of gene-specific mutations that destabilize the genome. Other types of genetic changes such as mutations of the p53 gene (Hartwell et al., 1994) or DNA mismatch repair genes (Fishel et al., 1995) also exist in progression part. Finally, tumor is developed following to the transformation of mutant DNA sequences causing progression from normal to cancerous type of cells.

Unfortunately, the process of the consequences of DNA mutations is not reversible. When a cell divides, accurate replication of 3 billion base pairs of its DNA is controlled by DNA proofreading and repair systems. However, if the gene contains cancer, errors during DNA replication and repair arise and hence, DNA remains unrepaired. Then, disruption and adaptation of cells to deregulated system of growing cancer occurs and cancer becomes dominant at that part of the body. Evolution of cancer from environmental risk factors is summarized in Figure 2.1 (Boyle et al., 2008).

An undesirable property of cancer cells is the loss of their adherence followed by their detachment from the tumor mass. The detached tumor cells enter the circulating blood and lymph and then transported to organs. As a result, cancer eventually spreads to other organs causing tumor development at those sites (tissues and organs). This process is called metastases (Takeichi, 1991).

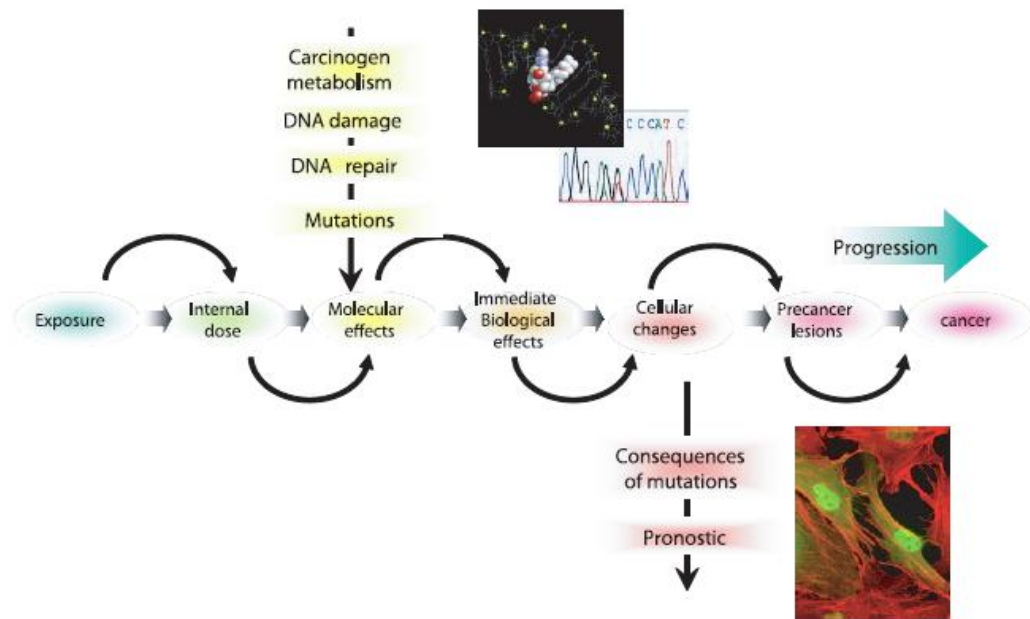


Figure 2.1. Evolution of Cancer from Environmental Risk Factors (Source: Boyle et al., 2008).

The choice of treatment (chemotherapy, radiotherapy or surgery) depends upon some factors such as cancer type, size, number and localization of metastases, age of the patient and the case if the patient has progressed cancer previously. The local treatment methods include surgery and radiotherapy. Radiotherapy is the use of 3-dimensional radiation on a very limited area of body (Fidler et al., 2007). Although certain cancer cells can be usually treated with radiotherapy, it is possible that some patients develop sensitivity to this therapy.

Surgery is applied to collect and remove the large cancerous tissues. Surgical techniques include laser surgery, cryosurgery, electrosurgery, mohs surgery and robotic surgery (Online Source, Special Surgical Techniques).

- Laser surgery: is a method where laser, a powerful beam of light energy, is used for cutting process. One advantage of this type of surgery is that less cut and damage become compared to standard surgery. Additionally, laser can also destroy the cancer site.

- Cryosurgery: is a technique in which a liquid nitrogen spray or a very cold probe is used to freeze and kill the cells. Cryosurgery can also be used as a treatment of pre-cancerous cells such as skin, liver and prostate cancers.
- Electrosurgery: is the use of electrical current to kill cancer cells and this technique might be applied to skin and mouth cancers.
- Mohs surgery: is also called as microscopically controlled surgery. Microscope is used to monitor the tissue after removing each cancer layer.
- Robotic surgery: is applied by robotic control and it can reduce the blood loss and pain after the surgery.

In surgical treatment methods, it is highly possible that after the removal of tumor, the residual cell is also affected such that growth rate might change. It is not feasible for undetectable cancer or cancer types, not confined in a solid tumor, like leukemia. Moreover, there is an infection risk and the recovery might be slow as it is an invasive process.

It is difficult to treat disseminated cancers. Therefore, in addition to localized therapies (surgery and radiotherapy), other systematic treatment methods such as chemotherapy and biological (hormone) therapies have been suggested. Biological therapies use monoclonal antibodies targeting the cells and prevent metastasis process whereas in chemotherapy, cytotoxic drugs are used to interfere with DNA and cancer cell division. Most of the chemotherapeutic agents are anthracycline antibiotics not preferred/used for the cure of bacterial infections. Indeed, they are DNA-damaging drugs by effecting the activities of topoisomerase I and topoisomerase II enzymes during transcription. Examples of these types of drugs are doxorubicin, daunomycin, camptothecin, epirubicin, and idarubicin.

In most cases, chemotherapy is an effective method as cancer cells replicate their DNA more often in order to divide and might be more sensitive than normal cells. In addition, cancer cells treated with chemotherapeutic agents usually die via apoptosis (controlled cell death). In Figure 2.2, human lymphoma (blood cell tumors) treated with a chemotherapeutic agent, camptothecin, is given. The cells that underwent apoptosis without inflammation appear yellowish and show membrane blebbing surfaces (Boyle et al., 2008).

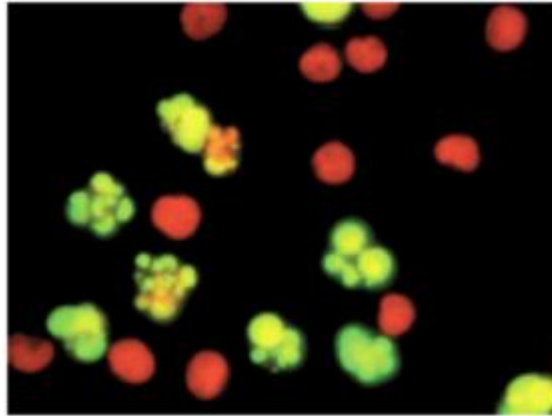


Figure 2.2. Human Lymphoma Exposed to Camptothecin
(Source: Boyle et al., 2008).

However, there are many side effects of chemotherapy on patients and some of them are listed below:

- Damage of healthy cells along with the cancer cells (as chemotherapeutic drugs cannot differentiate healthy and cancer cells)
- Hair loss
- Sickness and vomiting
- Anorexia and weight loss
- Tiredness and weakness
- Infection risk due to reduction of white blood cell.

2.2. Cancer Cell Properties and Ideal Drug Delivery Systems (DDS)

Due to the aforementioned side effects of toxic anticancer drugs, development of effective drug delivery systems is crucial to ensure the comfort of patients exposed to chemotherapy. Thus, an ideal drug delivery must be designed to carry sufficient drug with an ability to cross physiological barriers effectively and reach disease sites without allowing any activity loss of the drug. During the transit, there should be no leakage, by ensuring healthy cells not exposed to the drug. DDS must also possess high blood circulation time to achieve optimum therapeutic value at cancer sites. (Florence et al., 1993; Tong et al., 2007).

One of the targeting strategies used in the development of DDS is based on the unique property of cancer cells, enhanced permeability and retention (EPR) effect.

Compared to the normal cells, pore size of cancer cells is larger due to the leakiness of aberrant tumor endothelium. As a result, small molecules such as free drugs diffuse in and out of cancer cells, whereas nanoparticles are allowed to penetrate into tumor tissue and retained there. This property is called enhanced permeability and retention (EPR) effect (Figure 2.3). Thus, EPR effect is associated with macromolecular drugs entering into the tumor cells effectively from blood-stream and then accumulation inside the cell at high concentrations for prolonged time. The molar mass of drug or macromolecule-drug conjugates must be at or around its renal clearance threshold (40-45 kDa) for retention and accumulation inside the cell (Maeda et al., 1989; Tong et al., 2007; Kamaly et al., 2009). Indeed, polymer accumulation in tumor via EPR effect is quite more possible with increasing molar mass of polymer (Maeda et al. 2000). It was reported that EPR-mediated targeting was resulted in higher therapeutic activity of the drug due to retention and accumulation at cancer cell as expected (Veronese et al., 2005).

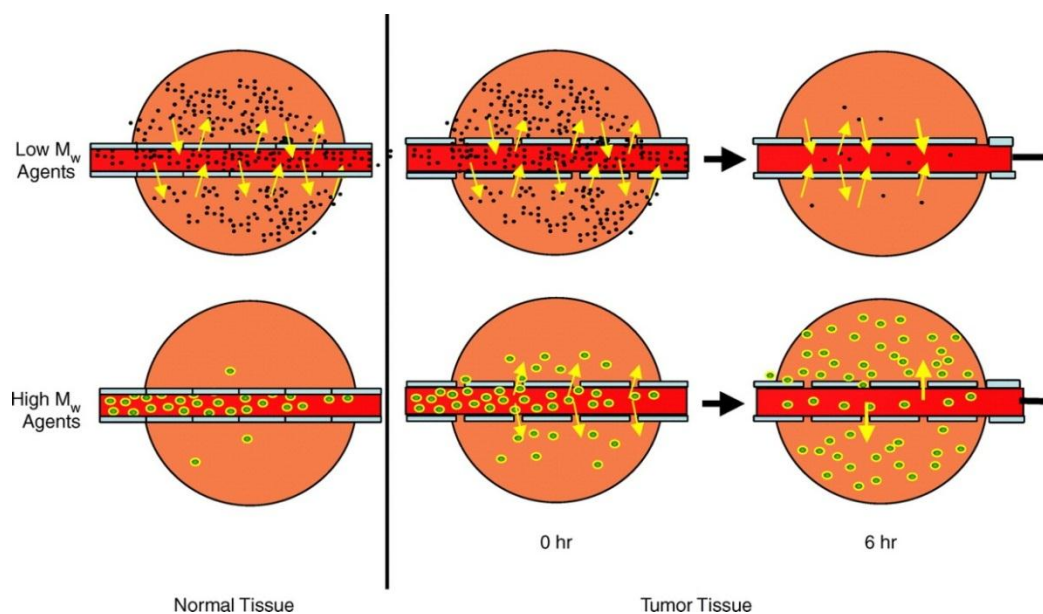


Figure 2.3. Illustration of EPR Effect
(Source: Fang et al., 2007).

Multidrug resistance (MDR) is a term describing resistance of tumor cells to cytotoxic effects of anti-cancer drugs resulted from changes in the plasma membrane or cellular compartments. MDR is associated with the changes in activity of variety of cellular proteins including P-glycoprotein (Pgp), a transmembrane efflux pump, and DNA topoisomerase II which functions to regulate DNA supercoiling. Overexpression

of the gene encoding Pgp (170 kDa) results in decrease in drug accumulation due to the activity of Pgp that pumps the drug outside of the cell (Noonan et al., 1990). Consequently, the cancer cells become less sensitive and do not respond to the drug at that site (Cole et al., 1992; Michael et al., 1993).

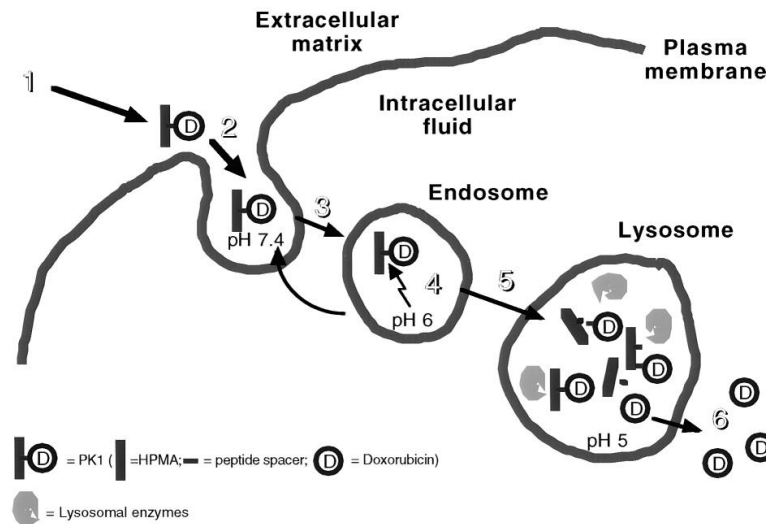


Figure 2.4. pH Programmed Drug Release at Cellular Compartments (Source: Engin et al., 1995).

To overcome MDR effect, DDS with fast release ability such as pH or temperature programmed manner have been proposed. pH gradient in the cellular compartments or slightly acidic tumor extracellular pH have been widely exploited in the development of so called pH responsive DDS (Vasey et al., 1999; Gillies et al., 2004).

In vivo extracellular pH (pH_e) was determined by Engin et al (1995). Mean tumor pH_e observed among adenocarcinoma, squamous cell carcinoma, soft tissue sarcoma and malignant melanoma was determined as 7.06 (5.66-7.78), whereas pH_e of normal tissue was estimated to be 7.33 ± 0.03 . On the other hand, pH gradient that starts with neutral cytoplasmic pH (7.4) and reduces to pH 6 and 5 in respective endosomal and lysosomal components offers more convenient pH programming (Engin et al., 1995; Lee et al., Nogueira et al., 2011; 2007; Tian et al., 2012). Mechanism of pH triggered release of a pH responsive DDS in endosomal compartments is given in Figure 2.4 (Engin et al., 1995).

2.2.1. DDS Based on Physical Interactions Between the Drug and Carrier

One of the widely employed strategies to prepare DDS is to attach drug to the carrier system via physical forces such as electrostatic or hydrophobic attractions. Perhaps, the most striking advantage of these systems is the conservation of the chemical identity of the drug intact. If ionizable groups are present, the carrier molecule may have pH responsive property as well.

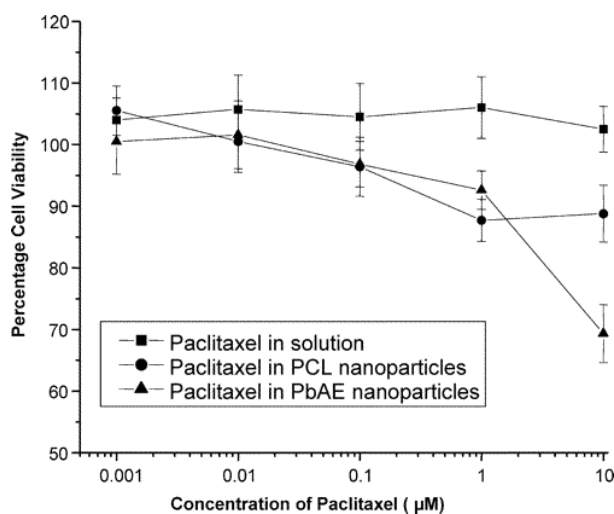


Figure 2.5. Comparison of the Cytotoxicity of Paclitaxel Loaded PCL and PbAE Nanoparticles (Source: Shenoy et al., 2005).

pH dependent solubility characteristics of poly- β -amino-ester (PbAE) have been exploited in the development of pH sensitive anticancer drug delivery systems. It was reported that PbAE is insoluble at physiological pH but the polymer can easily be dissolved in aqueous media when the pH of the solution is adjusted below 6.5. Additionally, PbAE is less toxic than poly(L-lysine) and can be synthesized using a simple route (Lynn et al., 2001; Akinc et al., 2003). These properties make PbAE a superb candidate in the development of pH responsive DDS. Shenoy et al., (2005) loaded paclitaxel to a PbAE-Pluronic F-18 blend and a non-pH responsive polymer, polycaprolactone (PCL) via solvent displacement method. Comparison of the cytotoxicity test of these two nanocarrier systems indicated that paclitaxel in pH responsive PbAE showed the highest therapeutic activity as given in Figure 2.5. It was suggested that pH responsive system composed of PbAE delivered the paclitaxel more

rapidly compared to PCL based systems by presenting faster anti-tumor activity (Shenoy et al., 2005).

In another study, paclitaxel was incorporated to pH responsive poly(β -amino ester)-graft-PEG polymer using solvent displacement or dialysis method. Drug release results given in Figure 2.6 indicated fast release at pH 5.0 as expected. However, there is also considerable paclitaxel release at pH 7.4 as well suggesting that this system may fail to deliver entire payload to tumor site efficiently (Shen et al., 2009).

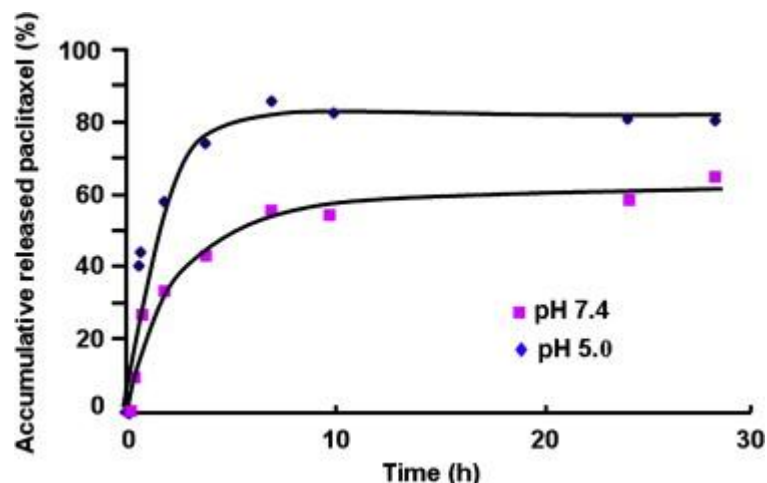


Figure 2.6. Paclitaxel Release of Poly(PbAE-g-PEG) at pH 5.0 and 7.4 (Source: Shen Y., 2009).

Similar to PbAE, poly(histidine) having an imidazole ring with ionization properties dictated by the solution pH has also been considered in the preparation of pH responsive DDS. The solubility of poly(histidine) depends on solution pH such that it is insoluble at neutral pH, whereas it becomes soluble below pH 6 (Pack et al., 2000).

Lee et al (2003) synthesized poly(L-His-block-PEG) and investigated its self-association behavior as a function of pH. The block copolymer micelles of (polyHis(5K)-b-PEG(2K)) with an average size of 114 nm were prepared by diafiltration process against borate buffer at pH 8.0. Critical micelle concentration (CMC) of the micelles was measured as 2.3 $\mu\text{g}/\text{mL}$ and reported to increase with increasing pH confirming pH responsive behavior of the copolymer.

In another study, pH programmed drug release properties of poly[(L-histidine)-co-(L-phenylalanine)]-block-poly(ethylene glycol) (HF-b-PEG) were determined using pyrene as a model component. Figure 2.7 suggests that poly(histidine) containing drug

delivery systems have potential by ensuring release of payload in endosomal compartments (Kim et al., 2005).

2.2.2. Drug Conjugated Delivery Systems

Drug delivery systems with covalently attached drugs may also exhibit pH responsive behavior by clever choice of the nature of the chemical bond between the drug and carrier molecule. Acetal, ketal, and hydrazone bonds with acid cleavable degradation properties, have been widely employed to ensure pH programmed release of the conjugated drug (Bae et al., 2003; Gillies et al., 2005; Heffernan et al., 2005; Zhou et al., 2011).

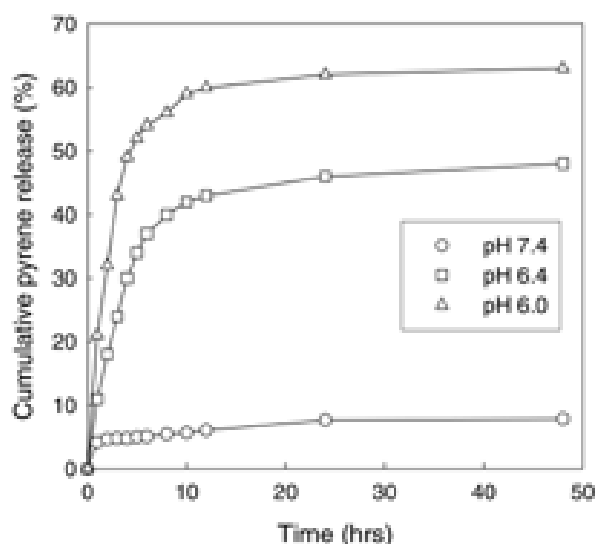


Figure 2.7. pH Programmed Release of Pyrene from poly(HF-b-PEG)
(Source: Kim et al., 2005).

Zhou et al. (2011) developed water soluble poly(ethylene oxide)-graft-doxorubicin (PEG-g-DOX) prodrugs, containing pH sensitive hydrazone linkage between the polymer and drug. DOX conjugated DDS was synthesized by applying three steps (i) anionic ring opening copolymerization of ethylene oxide (EO) and allyl glycidyl ether (AGE) (ii) transformation of allyl groups to hydrazide by reacting with methyl mercaptoacetate, followed by treating with hydrazine hydrate, (iii) conjugation of DOX to hydrazides via acid-labile hydrazone bond. Acid induced degradation of hydrozone bond can be clearly seen in the DOX release profile given in Figure 2.8. Based on these release profiles, drug release mechanism in the endocytosis pathway is

suggested as in Figure 2.9. Cytotoxicity of the conjugate system was determined using MTT assay. IC_{50} values were determined as 26.5, 42.5, and 32.0 μg DOX equivalent/ml for RAW 264.7, HeLa, and 4T1 breast tumor cells, respectively.

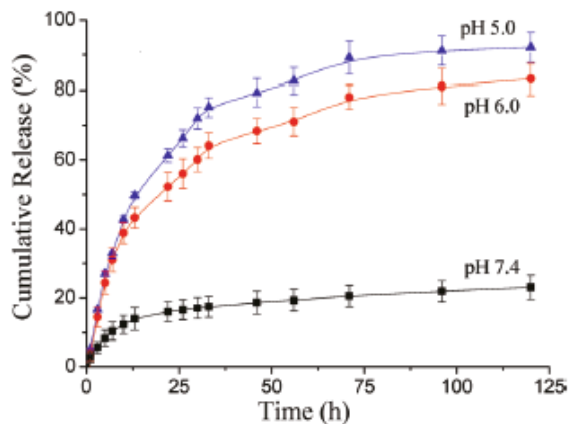


Figure 2.8. DOX Release Curves of PEG-g-DOX at Different pH Values (Source: Zhou et al., 2011).

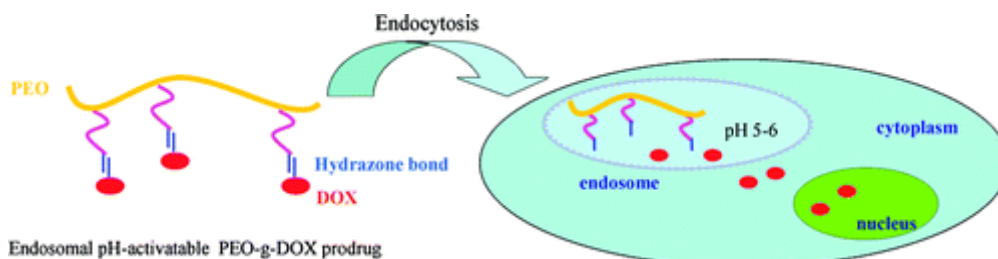


Figure 2.9. Endosomal Cleavage of Hydrazone Bond of a Prodrug (Source: Zhou et al., 2011).

pH sensitive amphiphilic block copolymer, poly(ethylene glycol)-poly(aspartate-hydrazone-adriamycin) (PEG-p(Asp-Hyd-ADR)) was synthesized by Bae et al. (2003). Synthesis procedure of adriamycin (DOX) conjugated block copolymer is given in Figure 2.10. DOX release profiles (Figure 2.11) indicated almost no release at physiological pH. However, compared to other systems DOX release at pH 5.0 was also low ($\sim 30\%$ at the end of 72 hrs). The DDS was reported to form aggregates with an

average size of ~65 nm. Therefore, it is likely that the aggregated structure of the DDS limits the diffusion of solvent molecules to reach hydrozone bond.

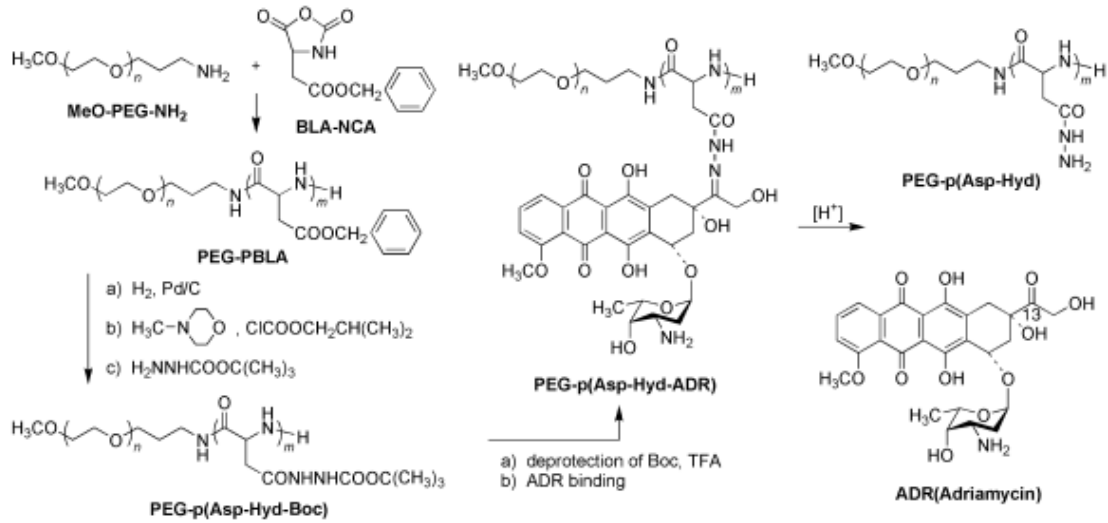


Figure 2.10. Synthesis of PEG-p(Asp-Hyd-ADR) Block Copolymers (Source: Bae et al., 2003).

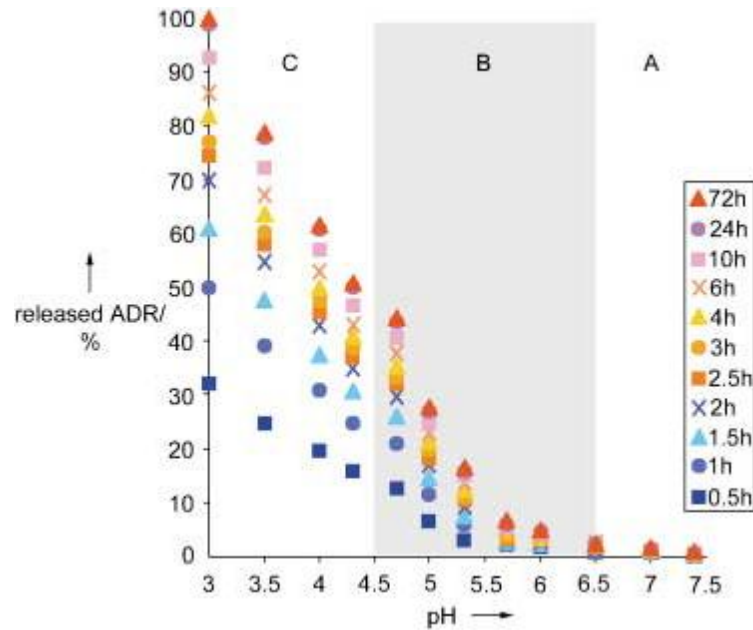


Figure 2.11. DOX Release from the PEG-p(Asp-Hyd-ADR) Block Copolymer (Source: Bae et al., 2003).

PEG-p(Asp-Hyd-ADR) block copolymers were reported to be highly toxic against SBC-3 cell line with an IC_{50} value of $0.27 \pm 0.038 \mu\text{g DOX equivalent/ml}$ (IC_{50} value of free DOX = $0.039 \pm 0.025 \mu\text{g/ml}$).

CHAPTER 3

MATERIALS AND METHODS

3.1. Materials

Methoxy polyethylene glycol-propionic acid (MW: 5000 g/mol with >80% COOH functionality), methoxy polyethylene glycol maleimide (MW: 5000 g/mol with >90% maleimide functionality), adipic acid dihydrazide (AADH), carbonyldiimidazole (CDI) and solvents, dimethyl sulfoxide (DMSO) and diethyl ether (DEE) were purchased from Sigma Aldrich. N-(3-Dimethylaminopropyl)-N'-ethylcarbodiimide hydrochloride (EDC.HCl) and N-Hydroxysuccinimide (NHS) were obtained from P3 Biosystems and Alfa Aesar, respectively. Synthesis grade trifluoroacetic acid (TFA) obtained from Merck-Millipore and doxorubicin HCl (DOX) purchased from Medkoo Biosciences were used for the drug conjugation reaction.

For peptide synthesis, rink amide MBHA resin, Fmoc-His-Trt-OH, Fmoc-Gly-OH, Fmoc-Cys-Trt-OH, Fmoc-Glu-(OtBu)-OH (NovaBiochem), HBTU, HOBt (P3 Biosystems) dimethyl formamide (DMF), dichloromethane (DCM), 4-Methylmorpholine (NMM) (Sigma-Aldrich), and piperidine (Acros) were used. Triisopropylsilane (TIS), 1,3-Dimethoxybenzene (DMB) and synthesis grade trifluoroacetic acid (TFA) (Merck) were employed in the cleavage reactions.

Sodium phosphate monobasic, imidazole (Fluka), sodium chloride, sodium hydroxide (Sigma Aldrich), anhydrous 4-Morpholineethanesulfonic acid (MES) (AppliChem), acetic acid and hydrochloric acid (Merck) were used in the preparation of buffers. His Pur Ni-NTA resin (Thermo Scientific) and Sephadex LH-20 (GE Healthcare) were employed in affinity and gel permeation chromatography, respectively. Snake Skin (MW 3.5 kDa) dialysis tubing (Thermo Scientific) was utilized in dialysis and drug release experiments.

Sinapic acid (Sigma), D₂O (Merck) and FTIR grade potassium bromide (KBr) (Sigma) were used in MALDI-TOF, NMR and FTIR spectroscopy sample preparations, respectively.

Gentamycin sulfate, European Grade Foetal Bovine Serum (FBS), Trypsin.EDTA Solution C and 0.5% Trypan blue solution were purchased from Biological Industries. RPMI-1640 with L-glutamine and 3-(4,5-Dimethylthiazol-2-yl)-2,5-Diphenyltetrazolium Bromide (MTT) were obtained from Sigma-Aldrich and Amresco, respectively.

All the chemicals and solvents were used without purification.

3.2. Methods

3.2.1. Preparation of Methoxy Polyethylene Glycol-Hydrazone-Doxorubicin (mPEG-HYD-DOX) Conjugates

The model anticancer drug, doxorubicin, was conjugated to the carrier molecule, propionic acid functionalized mPEG, via hydrazone bond using two steps:

- Synthesis of hydrazide form of the PEG
- Attachment of the drug

3.2.1.1. mPEG – HYD Synthesis

Hydrazide form of mPEG-propionic acid was prepared using EDC coupling reaction with dihydrazide molecules (AADH or CHYD) in the presence of NHS (Figure 3.1 and Figure 3.2). In a typical reaction, 1.5 mmol of AADH or CHYD (300 times excess with respect to COOH groups of mPEG-propionic acid) solution was prepared in 10 ml of PBS buffer with salt (100 mM of phosphate with 150 mM of NaCl) at pH 7.4 (Solution 1). For AADH reaction, the solution was sonicated at 40-45°C to ensure complete dissolution of the amine source. In a separate vial, 50 mg (5 µmol) of mPEG-propionic acid, 96 mg (0.5 mmol) of EDC.HCl, 46 mg (0.2 mmol) of NHS were

dissolved in 6 mL of 25 mM MES buffer containing 150 mM of NaCl at pH 6.0 (Solution 2). Next, the solution 2 was stirred at room temperature for ca. 15 min, and it was added onto solution 1 dropwise. After the solutions were combined, solution pH was adjusted to 7.4 and the reaction was allowed to proceed overnight at 30°C.

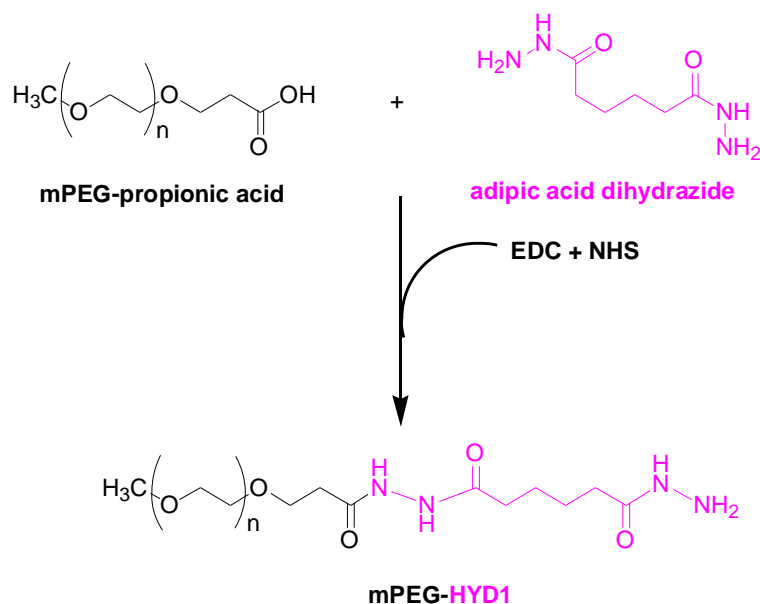


Figure 3.1. Reaction Scheme of mPEG-HYD1

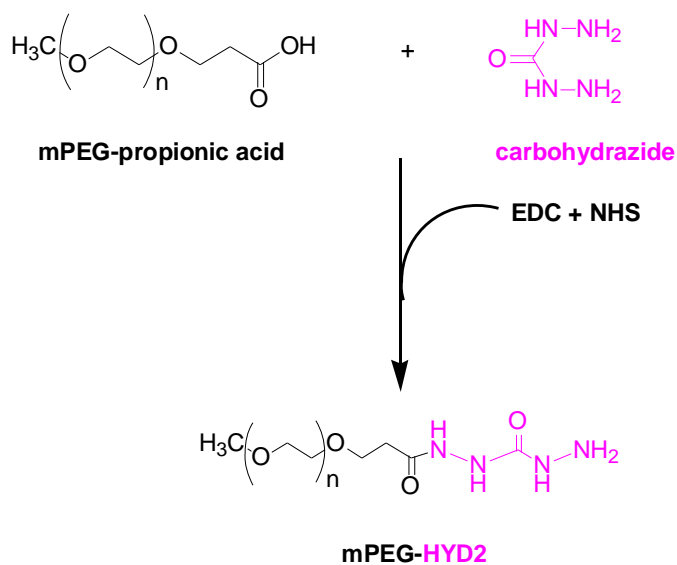


Figure 3.2. Reaction Scheme of mPEG-HYD2

To isolate mPEG compounds, the reaction mixture was first dialyzed against 2 L of 100 mM of phosphate buffer containing 150 mM of NaCl salt at neutral conditions.

The dialysis buffer was changed 3 times with 2 hours 4 hours and overnight intervals. On the following day, the product was further dialyzed against 4 L of deionized water to remove excess buffer components in addition to remaining small molecular weight excess reactants and by-products. The dialysis procedure continued for ca. 4 days with 3 changes of DI water per day. Conductivity of the solution in the dialysis membrane was checked to ensure the removal of buffer components. Dialysis was stopped when the conductivity reached below 10-15 $\mu\text{S}/\text{cm}$. The solution was afterwards freeze dried and the samples obtained were stored at -20°C . Yield of the final product (mixture of mPEG-propionic acid and mPEG-hydrazide) was obtained as $75 \pm 5 \%$. For mPEG-HYD1, hydrazide functionalization was determined as $53 \pm 1 \%$ using ^1H NMR. No further purification was applied prior to DOX conjugation.

3.2.1.2. Doxorubicin (DOX) Conjugation to mPEG-HYD

Ketone group of DOX was conjugated to the hydrazide of mPEG-HYD via the formation of acid cleavable hydrazone bond to obtain the final drug delivery system. Figure 3.3 and Figure 3.4 indicates conjugation reactions of DOX to mPEG-HYD1 and to mPEG-HYD2, respectively. DOX conjugation reactions were performed in DMSO using TFA as a catalyst at 30°C for 3 days (Bae et al., 2003). The reaction mixture was protected from light. A few reaction conditions were tested to determine the condition giving highest DOX conjugation percent (Table 3.1). In these preliminary reactions, 5 mg of mPEG-HYD1 (0.001 mmol) and 1 ml of DMSO were mixed and 2 or 4 mg (0.036 or 0.072 mmol) of DOX amount was added. Catalyst volume was used as 10 or 20 μl . Additionally, for sample S4, DOX was added to the reaction mixture twice: half at the beginning followed by half after the first day. The reaction condition giving the highest yield and DOX functionality was applied for synthesis of mPEG-HYD1-DOX and mPEG-HYD2-DOX conjugates.

Table 3.1. DOX Conjugation Experiments

Sample Code	mPEG- HYD1 : DOX (mg/mg)	DOX addition type	TFA (μ l)
S1	2.5:1	single	10
S2	2.5:1	single	20
S3	2.5:2	single	20
S4	2.5:2	twice	20

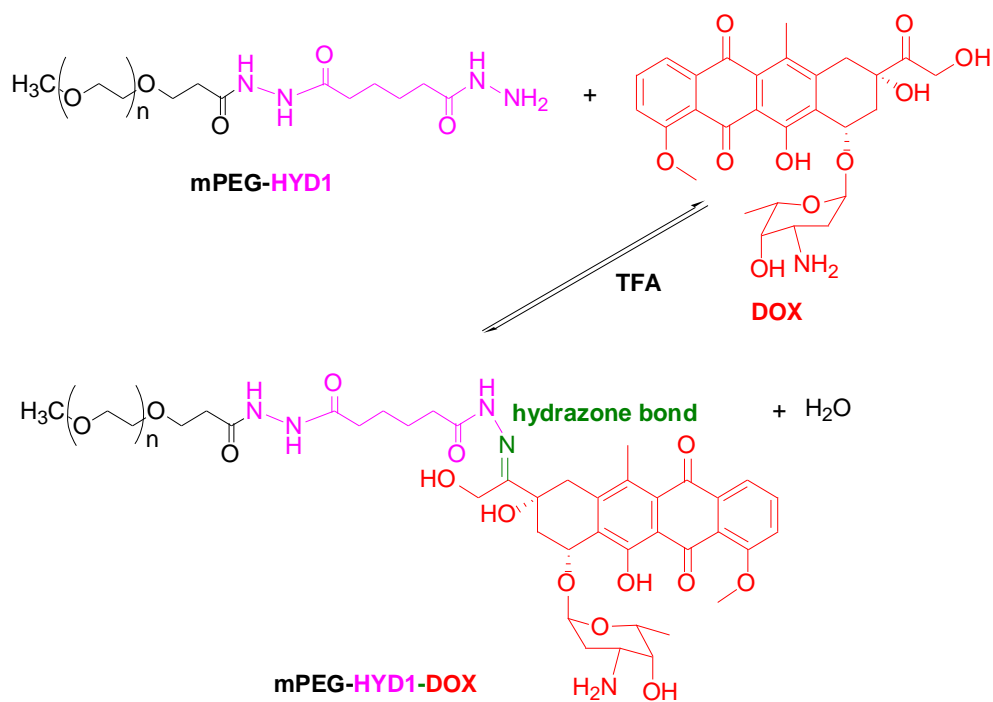


Figure 3.3. Conjugation Reaction of DOX to mPEG-HYD1

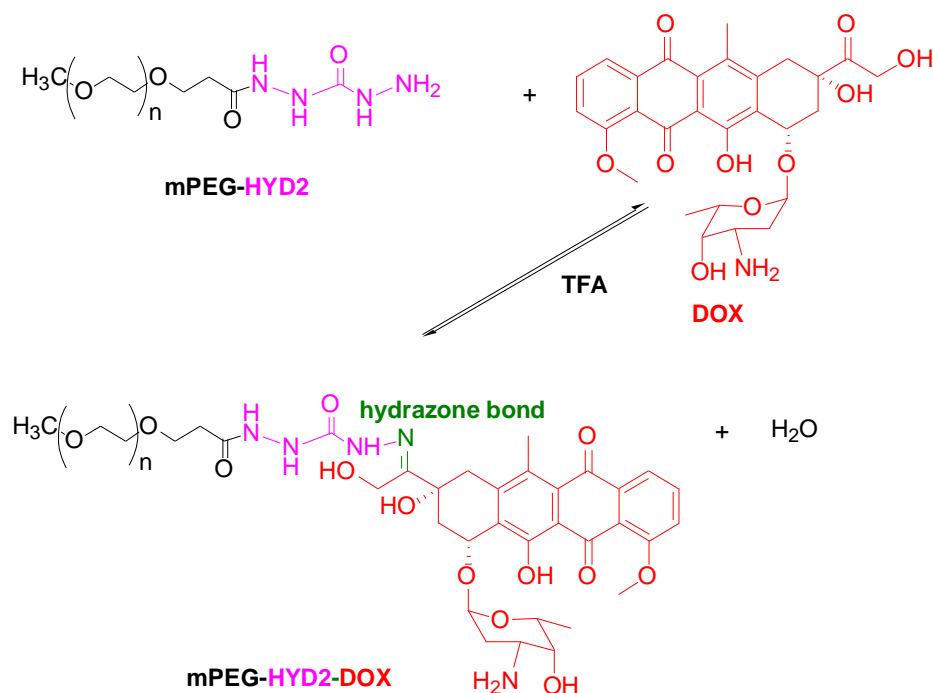


Figure 3.4. Conjugation Reaction of DOX to mPEG-HYD2

After the reaction was completed, conjugates were precipitated over cold (stored at $-20\text{ }^{\circ}\text{C}$) DEE. Samples were centrifuged to obtain the pellets containing mainly mPEG-DOX conjugates. The supernatant corresponded to some portion of free DOX as depicted from orange color. Residual DEE was removed by allowing the conjugate to dry for a few hours in a fume hood. Gel permeation chromatography was applied to remove remaining free DOX using Sephadex LH-20 resin suspended in DMSO. In the elution fractions, mPEG-DOX conjugate was obtained first followed by unreacted DOX due to the size difference. Then, the isolated conjugates were precipitated onto cold DEE to get rid of DMSO. DEE was evaporated in a fume hood. Finally, the conjugates were dissolved in deionized-water, freeze dried and stored at -20°C .

3.2.2. Preparation of mPEG-Peptide-HYD-DOX Conjugate

mPEG-peptide-HYD-DOX conjugate system was prepared using 4 steps:

- Peptide synthesis
- Conjugation of mPEG and peptide
- Synthesis of hydrazide form of the mPEG-peptide

- Attachment of the drug

3.2.2.1 . Peptide Synthesis

The peptide, [Cysteine-(Glycine)₃-(Histidine)₆-(Glycine)₃-(Glutamic acid)], CGGGHHHHHGGGE was synthesized by employing Fmoc strategy on the rink amide MBHA resin (0.66 mmol/g functionality). Solid Phase Peptide Synthesis (SPPS) was carried out using an automated peptide synthesis instrument (AAPTEC Focus XI). Deprotection reactions were performed using 20% piperidine in DMF for 15 min and were repeated three times. Coupling reactions were carried out using HBTU and 0.4 M NMM as activating agents for 1 hr. In addition to these agents, HOBT was also used during the coupling of Histidine (His) and Cysteine (Cys) residues to prevent racemization. For each aminoacid, double coupling cycles were performed. At the end of the synthesis, the resin was washed with DCM and dried under N₂ flow at room temperature. Cleavage reactions were conducted using 92.5:5:2.5 TFA:DMB:TIS cocktail for 2.5 hours. The resin was filtered using a polypropylene column and the supernatant was precipitated over cold DEE with 1:10 cleavage cocktail: DEE ratio. The precipitate was washed with DEE and centrifuged twice. After evaporation of DEE under N₂ flow at room temperature, the raw peptide was dissolved in 1-2 ml of 1% acetic acid in deionized water, freeze dried and stored at -20°C.

3.2.2.2. mPEG-Peptide Synthesis

PEGylation of the raw peptide was carried out using Michael addition reaction involved in the mPEG-maleimide and thiol group of cysteine at the N-terminus of the peptide (Figure 3.5). Approximately, 20 mg peptide (0.014 mmol) was dissolved in 10 ml of PBS buffer (100 mM of phosphate buffer with 150 mM of NaCl at pH 7.2) under nitrogen gas for 10 min to prevent air oxidation of cysteines. 75 mg (0.015 mmol) of PEG-MAL was added under N₂ blanketing and the reaction was allowed to proceed for 4 hours. Unreacted mPEG-MAL was separated using affinity chromatography using Ni-NTA resin which selectively binds to histidines of the peptide and mPEG-peptide conjugate.

For the affinity chromatography, 50 mM phosphate containing 0.3 M NaCl at pH 8.0 was used as binding and washing buffer. Unbound mPEG-MAL was washed away until no PEG was detected in the solution by applying a colorimetric assay based on the complex formation of barium iodide and PEG. The peptide and mPEG-peptide, on the other hand, were eluted from the resin using 50 mM phosphate containing 0.3 M NaCl and 0.5 M imidazole at pH 7.4 buffer. PEG content of the elution fractions was determined by the colorimetric test above. In this method, 4 μ l of sample (wash or elution fractions) was placed into a glass vial and diluted with 40 μ l of deionized water. Then, 10 μ l of BaCl₂ (5% (w/v) barium chloride in 1 M HCl) solution and 5 μ l of iodine (1.27 g was iodine in 100 ml of 2% (w/v) KI) solution was added sequentially and shaken. Brown color indicates the presence of PEG, whereas light yellow color (matches to the color of the blank solution) suggests no detectable PEG in the solution (Gong et al., 2007).

To isolate mPEG-peptide conjugate, the peptide was removed by dialysis against deionized water using SnakeSkin dialysis tubing membrane with MWCO 3000Da. Dialysis continued until the conductivity of the solution in the membrane reduced to 10 μ S/cm. Finally, the conjugate was freeze-dried and stored at -20°C.

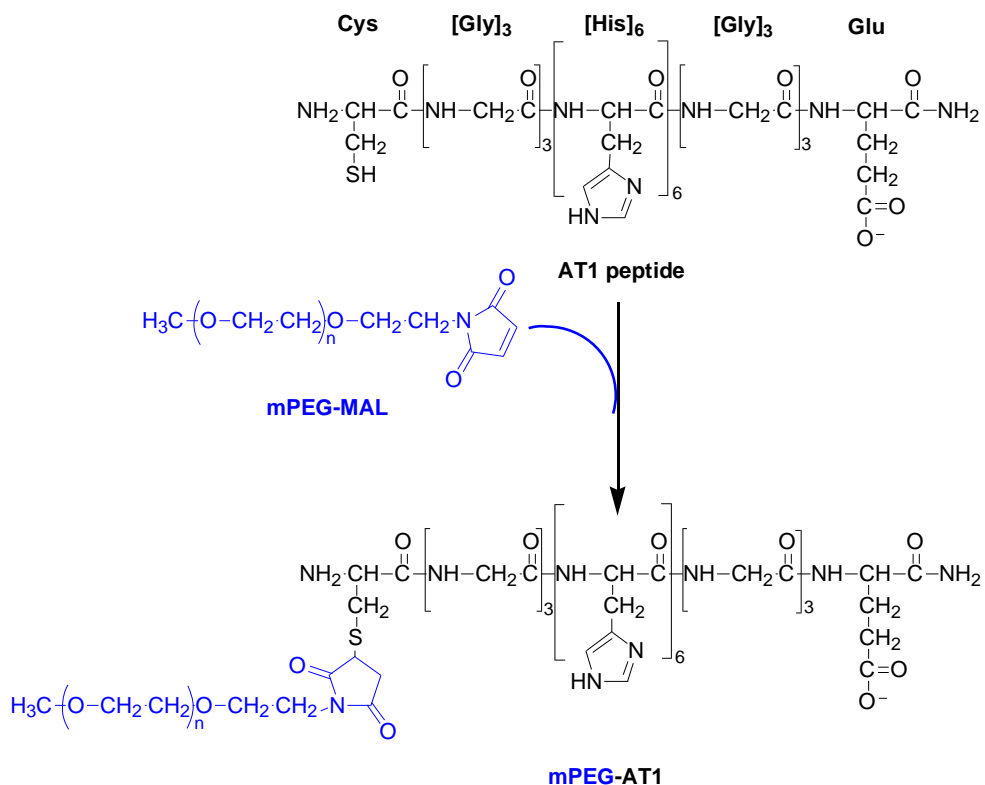


Figure 3.5. Reaction Scheme of mPEG-AT1

3.2.2.3. mPEG -Peptide -DOX Conjugate Synthesis

Same experimental procedures as described in Section 3.1.1.1 and 3.1.1.2 were applied to obtain hydrazide form and DOX conjugated form of mPEG-peptide respectively. The reaction schemes are shown in Figure 3.6 and Figure 3.7. Basically, mPEG-peptide-HYD conjugate was formed by the reaction between AADH and carboxylic group of glutamic acid residue at the C-term of the peptide. DOX conjugation reaction was carried out using 2.5 mg : 2 mg mPEG-Peptide-HYD1 : DOX ratio with 20 μ l of TFA per 1 ml of DMSO. DOX was added at the beginning of the reaction and the reaction was allowed to continue for 3 days at 30 $^{\circ}$ C at 120 rpm.

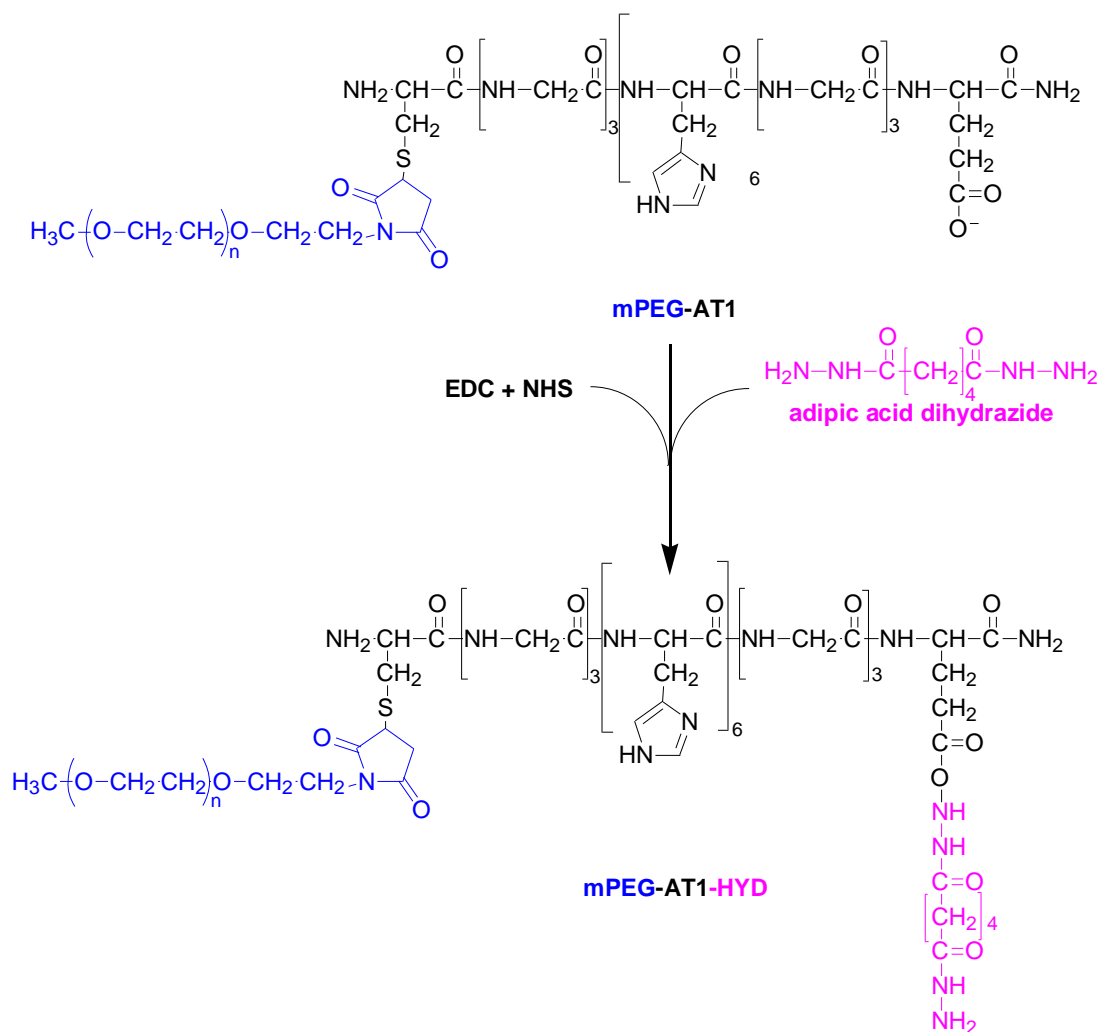


Figure 3.6. Synthesis of mPEG-AT1-HYD

3.3. Characterization

3.3.1. NMR Analysis

~ 2.5 mg of sample was dissolved in 0.6 ml of D₂O and ¹H NMR spectrum was taken using Varian VNMR 400 model spectrometer. NMR data were analyzed using ACDLAB 12, 1D NMR Processor software.

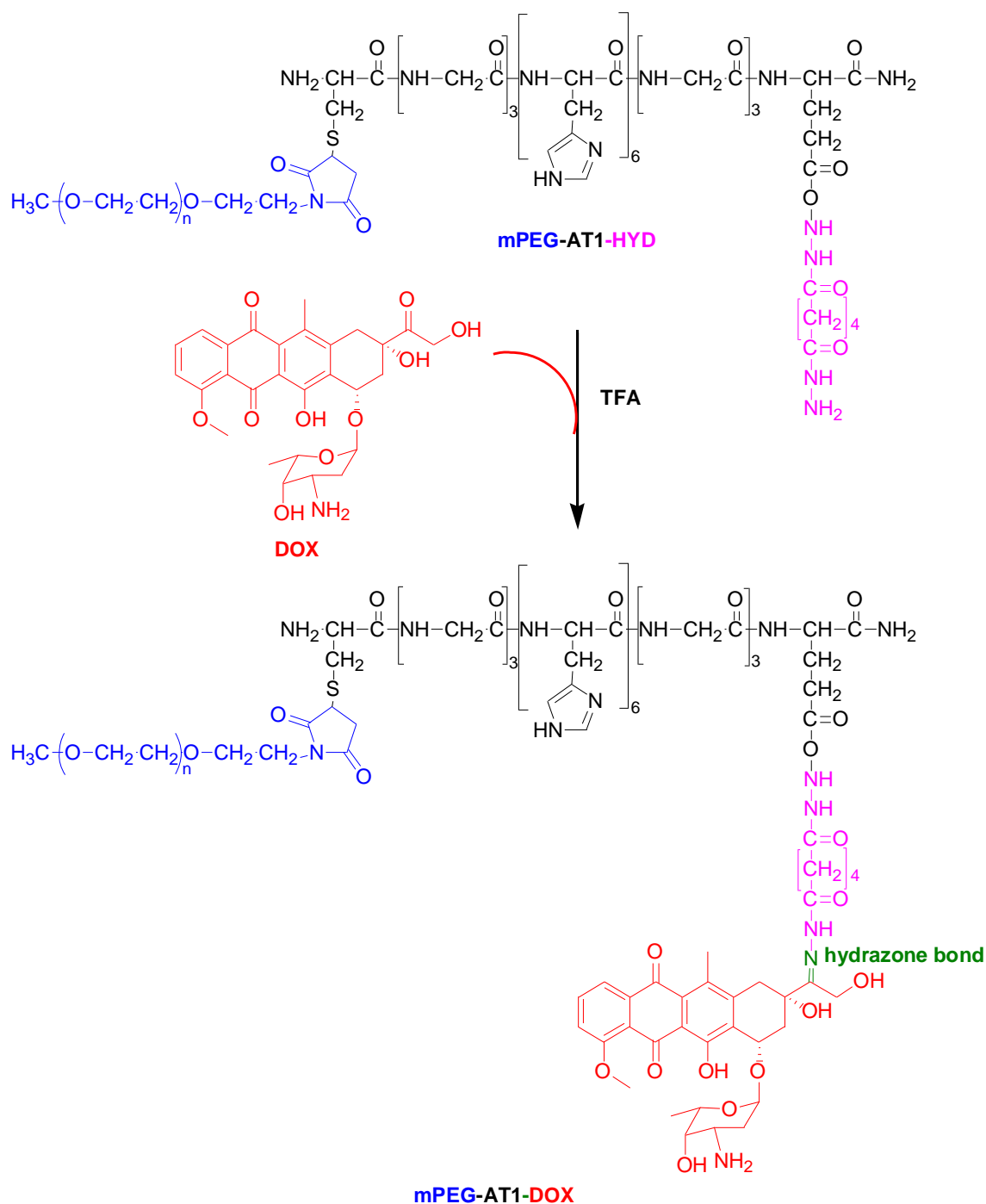


Figure 3.7. Reaction Scheme of mPEG-AT1-DOX

3.3.2. Fourier Transform Infrared Spectroscopy (FTIR) Analysis

FTIR analysis was conducted using KBr pellet technique. Prior to analysis, moisture of samples was removed/reduced using a vacuum oven at room temperature. Approximately 1 mg of sample was dispersed in 150 mg of potassium bromide (KBr).

The spectra were taken between 400-4000 cm^{-1} by using Shimadzu IRPrestige-21 FTIR-8400S Model Spectrophotometer.

3.3.3. High Performance Liquid Chromotography (HPLC)

Purity of samples was determined by Agilent 1100 Model HPLC system. 100 μl of filtered sample prepared in 0.1% TFA in water (~1-2 mg/ml) was injected to C18 analytical column. In the reverse phase HPLC method, 0.1% TFA in water and 0.08% TFA in acetonitrile were used as Solvent A and Solvent B respectively. Solvent A:B ratio was changed from 95:5 to 30:70 within 65 min and the sample eluted from the column was monitored at 214 nm using a UV detector. Analyses were carried out at 1 ml/min solvent flow rate.

3.3.4. Mass Spectroscopy

Mass spectroscopy of the samples was taken at Biological Mass Spectrometry and Proteomics Facility located at the Chemistry Department of İzmir Institute of Technology. Molar mass of the peptide was determined using electrospray ionization mass spectroscopy (ESI-MS). The experiments were performed with an LTQ XL linear ion-trap mass spectrometer (Thermo Finnigan, San Jose, CA) equipped with an electrospray ionization source. The solid peptide samples were dissolved in 1 % acetic acid containing ultra-pure water and mixed with equal proportion with HPLC-grade methanol and infused directly into the mass spectrometer.

Matrix-assisted laser desorption/ionization time of flight mass spectroscopy MALDI-TOF-MS was used for identification of the mPEG-peptide conjugate. The experiments were conducted. The sample was dissolved in 0.1% TFA in water and sinapic acid was used as matrix.

3.3.5. UV Vis Spectroscopy

DOX conjugation percentages of the conjugates (mPEG-HYD1-DOX, mPEG-HYD2-DOX, mPEG-Peptide-HYD1-DOX) were determined using Perkin Elmer Lambda-45 model UV-Vis spectroscopy. Approximately 0.5 mg conjugate was dissolved in 700 μ l DI water. The exact concentration was recorded for further calculations. Absorbance value of the solution was determined at 488 nm and DOX functionalization of the samples were calculated based on the extinction coefficient of free DOX ($11500 \text{ L}\cdot\text{mol}^{-1}\cdot\text{cm}^{-1}$) using the following equations:

$$\% \text{ DOX conjugation} = \frac{C \left(\frac{\text{mmol}}{\text{ml}} \text{ of DOX measured} \right)}{C \left(\frac{\text{mmol}}{\text{ml}} \text{ of the conjugate} \right)} \times 100\% \quad (3.1)$$

$$C \left(\frac{\text{mmol}}{\text{ml}} \text{ of DOX measured} \right) = \frac{\text{Absorbance measured at 488 nm}}{11500 \frac{\text{ml}}{\text{mmol cm}} \times 1 \text{ cm}} \quad (3.2)$$

$$C \left(\frac{\text{mmol}}{\text{ml}} \text{ of the conjugate} \right) = \frac{\text{Mass concentration of the conjugate} \left(\frac{\text{mg}}{\text{ml}} \right)}{\text{MW of the conjugate} \left(\frac{\text{mmol}}{\text{mg}} \right)} \quad (3.3)$$

3.3.6. Size Measurement

The size of the conjugates was determined using Malvern ZetaSizer Nano ZS model instrument via dynamic light scattering technique. Diffusion coefficients of the samples were estimated by applying CONTIN method and the diffusion coefficient values were converted to the hydrodynamic diameter via Stoke-Einstein equation provided by the software. 3 mg/ml of the samples were dissolved in deionized water and diluted 2 times with 20 mM phosphate buffer with 300 mM NaCl at pH 7.4 or 20 mM acetate buffer with 300 mM NaCl at pH 5.0 and filtered. The measurements were performed within a few hours after preparation of the solutions and after incubating the solutions for overnight at 37°C. The measurements were performed after equilibrating the cuvette for at least 2 min at 25°C and were repeated three times.

3.3.7. Drug Release

Drug release profile was obtained using dialysis procedure (Song et al., 2015, Lee et al., 2003). ~ 1.5 mg sample dissolved in 1 ml of buffer (10 mM acetate buffer with 150 mM NaCl at pH 5.0 or 10 mM phosphate buffer with 150 mM NaCl at pH 7.4) was placed in a dialysis bag with a MWCO of 3.5 kDa (Zhang et al., 2016). The membrane was transferred to a 50 ml Falcon tube containing 25 ml of buffer solution and the cover of the tube was wrapped with parafilm to prevent evaporation. The tube was incubated at 37°C by shaking at 150 rpm. 200 µl of solution was withdrawn and replaced with the same volume of fresh buffer at certain intervals (1, 3, 6, 10, 24, 48, 56, and 72 hrs). Released DOX amount was determined via fluorescence measurements at 590 nm using calibration curves of free DOX prepared at the same experimental conditions (Figure A.1 and A.2). Fluorescence measurements were performed on a Perkin Elmer LS55 model fluorescence spectrophotometer using excitation wavelength as 480 nm, excitation slit width as 5 nm, emission slit width as 20 nm and scan rate as 125 nm/min. Emission spectrum was recorded between 400-700 nm. DOX % released was determined using the following equations:

$$DOX \text{ released } \% = \frac{C_t \text{ (mmol of DOX released at time } t\text{)}}{C_i \text{ (mmol of DOX in the conjugate initially)}} \times 100\% \quad (3.4)$$

$$C_i = \frac{1.5 \frac{mg}{ml} \text{ conjugate} \times 1ml}{MW \text{ of the conjugate } \left(\frac{mg}{mmol} \right)} \times \frac{DOX \text{ conjugation } \%}{100 \%} \quad (3.5)$$

$$C_t = \frac{\text{Fluorescence intensity at } 590 \text{ nm}}{\varepsilon_{590} \left(\frac{ml}{mmol \text{ cm}} \right) \times 1 \text{ cm}} \times 25 \text{ ml} \quad (3.6)$$

where ε_{590} is the slope of the calibration curve. Sample calculation is given in Appendix A.

3.3.8. Cytotoxicity Test

Cytotoxicity tests were carried out using MTT assay on lung cancer cell lines (A-549) after ensuring the growth of cells in a plate and observing that the cells possessed the desired morphology. The morphology with convenient confluency (>80% by area of cancer cells) and growth curve of A-549 were shown in Figure A.3.

In a typical MTT assay, 90 μl aliquots of the cells (5×10^3) cells/well were seeded (number of replicates = 4) in a 96 (8 x12) well microplate. Then, the cells were incubated at 37°C in 5% CO_2 atmosphere for 24 h. At the end of the incubation period, 10 μl of sample (both conjugates and controls) in sterile PBS was added at various concentrations (0.5-1000 $\mu\text{g}/\text{ml}$ for DOX and 0.75-15000 $\mu\text{g}/\text{ml}$ for the other samples) (Table A.1). The cells were incubated for another 24 h at the same conditions. After 24 h, medium was discarded and changed with the fresh medium, then incubated for 24 h again (Bae et al., 2003) prior to application of MTT assay. In the first step, 10 μl of 5 mg/ml MTT in sterile PBS was added and the microplates were further incubated for 3 hrs. After centrifuging at 1800 rpm and at room temperature for 5 min, the medium was removed by a pipette, the microplate was inverted and blotted with a napkin. Next, 100 μl of DMSO was added and the microplates were shaken at 150 rpm for 5 min. Absorbance values were recorded at 570 nm with a reference wavelength of 690 nm using VarioSkan Flash Multimode Reader (Thermo Scientific).

MTT cell viability test is a colorimetric assay based on the metabolic activity of mitochondrial dehydrogenase, which converts tetrazolium salts to the purple formazan crystals via the reaction given in Figure 3.9. Therefore, viable cells give higher absorbance value (darker purple color) and % viability can be calculated easily using:

$$\text{viability \%} = \frac{\text{Absorbance of the sample at 570 nm}}{\text{Absorbance of the control (PBS) at 570 nm}} \times 100\% \quad (3.7)$$

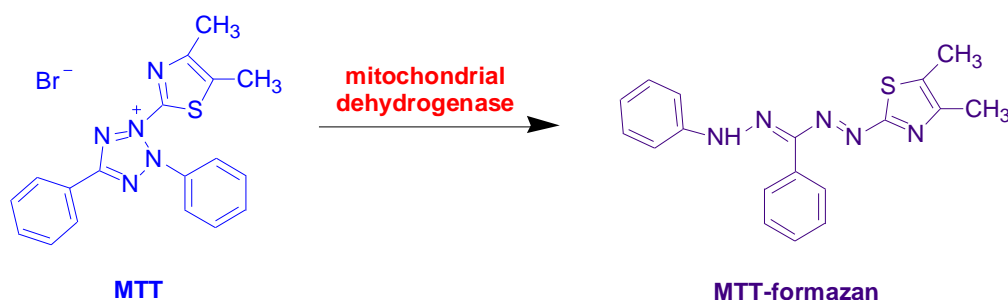


Figure 3.8. Conversion of Tetrazolium Salt to Formazan Crystals

IC_{50} values of the samples were estimated as the concentration that corresponds to 50% cell viability. Finally, DOX equivalent IC_{50} values of the conjugates were calculated as:

$$DOX \text{ equivalent } IC_{50} \text{ value} = \frac{IC_{50} \text{ value of the conjugate} \times MW_{DOX} \left(\frac{g}{mol} \right) \times DOX \text{ conjugation } \%}{MW_{conjugate} \left(\frac{g}{mol} \right)} \quad (3.8)$$

where the unit of IC_{50} value of the conjugate is $\left(\frac{\mu g \text{ conjugate}}{ml} \right)$.

CHAPTER 4

RESULTS AND DISCUSSIONS

4.1. Preparation of PEG Based DDS

In the first step of the preparation of hydrazone bonded DOX conjugates, hydrazide functionalized mPEG molecule was synthesized using EDC and NHS activated carboxylic acid-hydrazide coupling reaction. Hydrazide groups have been introduced to the carrier molecules via different routes. For example, Etrych et al. (2001) obtained hydrazide functionalized N-(2-hydroxypropyl) methacrylamide (HPMA)-methacryloyl glycyglycine 4-nitrophenyl ester (Ma-Gly-Gly-ONp) random copolymers using the reaction between 4-nitrophenoxy (ONp) group and hydrazine monohydrate in methanol (Etrych et al., 2001). In the other study, hydrazide groups were conjugated to aspartic acid side chains of mPEG-polyaspartate block copolymers in tert-butyloxycarbonyl (BOC) protected form via acid anhydride reaction in the presence of N-methylmorpholine (NMM), isobutyl chloroformate (IBCF), carbazic acid tert-butyl ester (Cat-BE) and dimethyl acetamide (DMAC). The protecting BOC group was then removed using TFA to obtain hydrazide functionalized form of the block copolymer (Bae et al., 2003). Hydrazide form of a PEG copolymer containing allyl groups were prepared using two consecutive reactions including the reaction with methyl mercaptoacetate in the presence of AIBN in THF followed by the reaction with hydrazine hydrate in THF (Zhou et al., 2011)

In this study, on the other hand, simpler route performed in aqueous medium was proposed by modifying the procedure given in Hermanson (1997). It was possible to use commercially available mPEG-hydrazide for DOX conjugation but in long term, hydrazide modification would be necessary when peptide or polypeptide was incorporated to the carrier system. For this reason, propionic acid form of mPEG (mPEG-COOH) was used to mimic the hydrazide functionalization reaction of carboxylic groups of glutamic acids in peptides/polypeptides. In the reaction used in current study, EDC.HCl acts as a zero length crosslinker to couple carboxyl groups of

mPEG-COOH to primary amine group of a dihydrazide molecule forming an amine reactive O-acylisourea as an intermediate product. It was reported that in the presence of water, the yield of amide formation is low because of the fast hydrolysis rate ($2-3 \text{ s}^{-1}$) of O-acylisourea (Hoare et al., 1967). Introduction of NHS, stabilized this intermediate molecule and yielded formation of amine reactive sulfo-NHS ester, which was more stable towards hydrolysis (Conde et al., 2014) (Figure A.4). Two different dihydrazide components, adipic acid dihydrazide (AADH) and carbohydrazide (CHYD) were used as amine sources forming the respective hydrazide forms, mPEG-HYD1 and mPEG-HYD2.

Hydrazide functionalization of mPEG was monitored using FTIR spectroscopy qualitatively. FTIR spectra of mPEG-propionic acid, mPEG-HYD1 and mPEG-HYD2 were given in Figure 4.1 and those of AADH and CHYD were shown in Figure A.5 in Appendix for comparison. FTIR spectra of AADH and CHYD indicated N-H bending band around $1630-1640 \text{ cm}^{-1}$. In the FTIR spectrum of mPEG-propionic acid, characteristic C-O stretching band of ether backbone was observed at 1110 cm^{-1} . The bands around 1465 and 2885 cm^{-1} were due to the respective bending and stretching of C-H groups. A weak band observed at 1727 cm^{-1} corresponded to carbonyl group. In the hydrazide functionalized samples, on the other hand, this band disappeared. In addition to the bands observed for mPEG-propionic acid, a new band around $1655-1665 \text{ cm}^{-1}$ attributed to N-H bending suggesting the hydrazide functionalization reaction was successful.

To get the quantitative information about hydrazide conjugation, ^1H NMR spectroscopy was obtained. NMR spectra of AADH, mPEG-propionic acid, and mPEG-HYD1 samples in D_2O are given in Figures A.4, Figure 4.2 and Figure 4.3. Theoretical chemical shift values of the reactants and products are shown in Table A.2 in Appendix A. In the NMR spectrum of AADH, chemical shifts observed at 1.53 and 2.17 ppm belong to CH_2 groups and consistent with the theoretical chemical shift values. The area values corresponding to 4 protons of these shifts were found to be consistent and proportional (Figure A.6).

NMR spectrum of mPEG-COOH exhibited a singlet at 3.31 ppm due to 3 protons of $\text{CH}_3\text{-O}$ (methoxy) groups and the area of this chemical shift was set to 3 to do quantitative analysis. A large peak observed at 3.64 ppm was related to the ether

backbone protons ($\text{O-CH}_2\text{-CH}_2$)_n and the number of protons was 4 times number of repeating units in PEG. By using the area of those protons, number average molecular weight (M_n) of mPEG-COOH was obtained as ~ 5400 Da (theoretical value = 5000 Da). The chemical shift at 2.62 ppm was due to 2 protons next to carboxylic acid group and using the area of this peak, percentage of COOH functional group was calculated as 88% (spect. value > 80%).

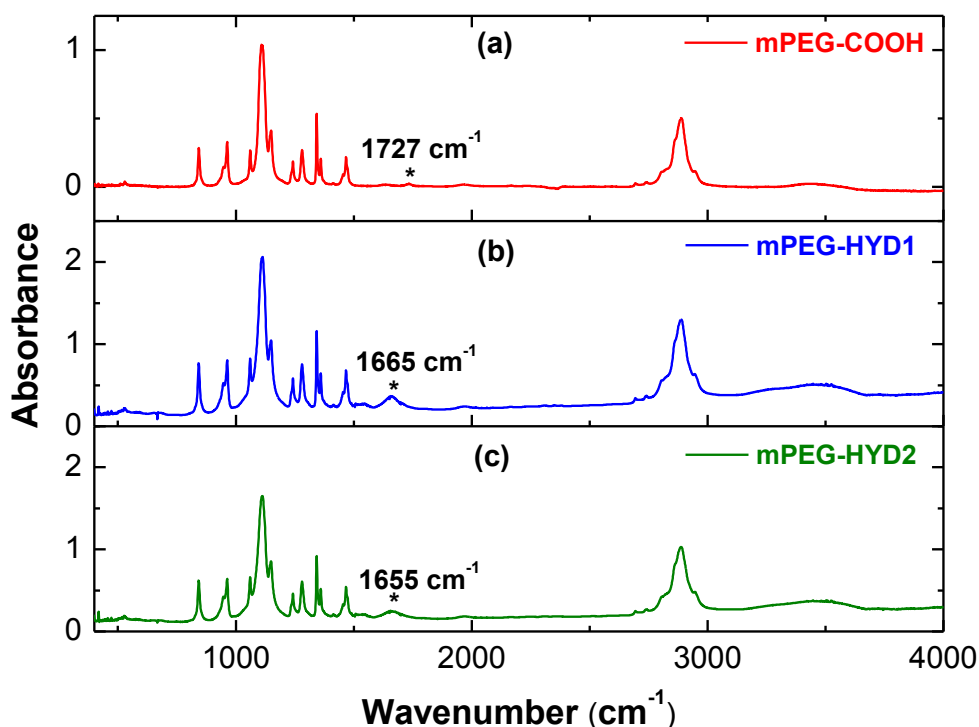


Figure 4.1. FTIR Spectra of mPEG-Propionic Acid, mPEG-HYD1 and mPEG-HYD2

In the NMR spectrum of mPEG-HYD1, chemical shift of CH_2 protons at 1.53 ppm observed in the NMR spectrum of AADH shifted to 1.56 ppm as can be seen in Figure 4.3. Other CH_2 chemical shifts expected around 2.2 ppm were merged with the chemical shift observed at 2.62 ppm originated from the parent mPEG-COOH molecule making this region complicated for the quantitative analysis. For this reason, the area of chemical shift at 1.56 ppm only was used to determine hydrazide functionalization percentage. Similar to the quantitative analysis of mPEG-COOH, area of the chemical shift at about 3.3 ppm was set to 3 and number average molecular weight of polymer was determined from the area of protons under 3.63 ppm chemical shift. M_n of mPEG-HYD1 was estimated as 5500 Da close to that of the mPEG-COOH.

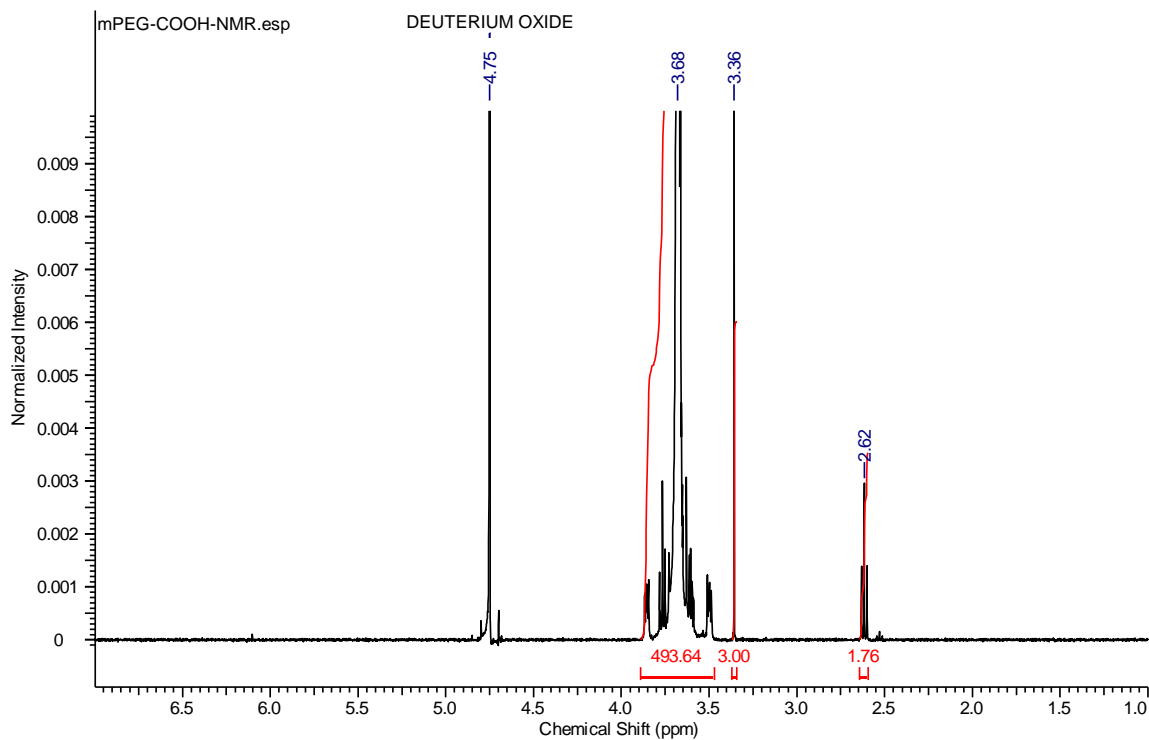


Figure 4.2. NMR Spectrum of mPEG-COOH in D₂O

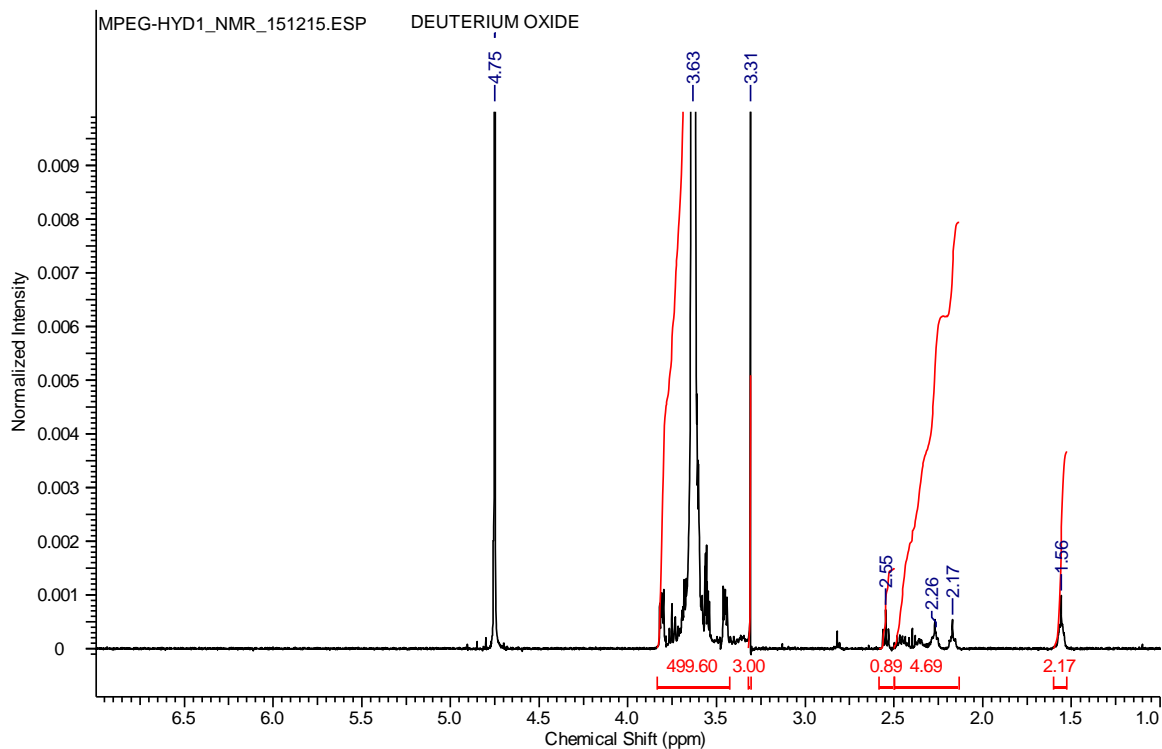


Figure 4.3. NMR Spectrum of mPEG-HYD1 in D₂O

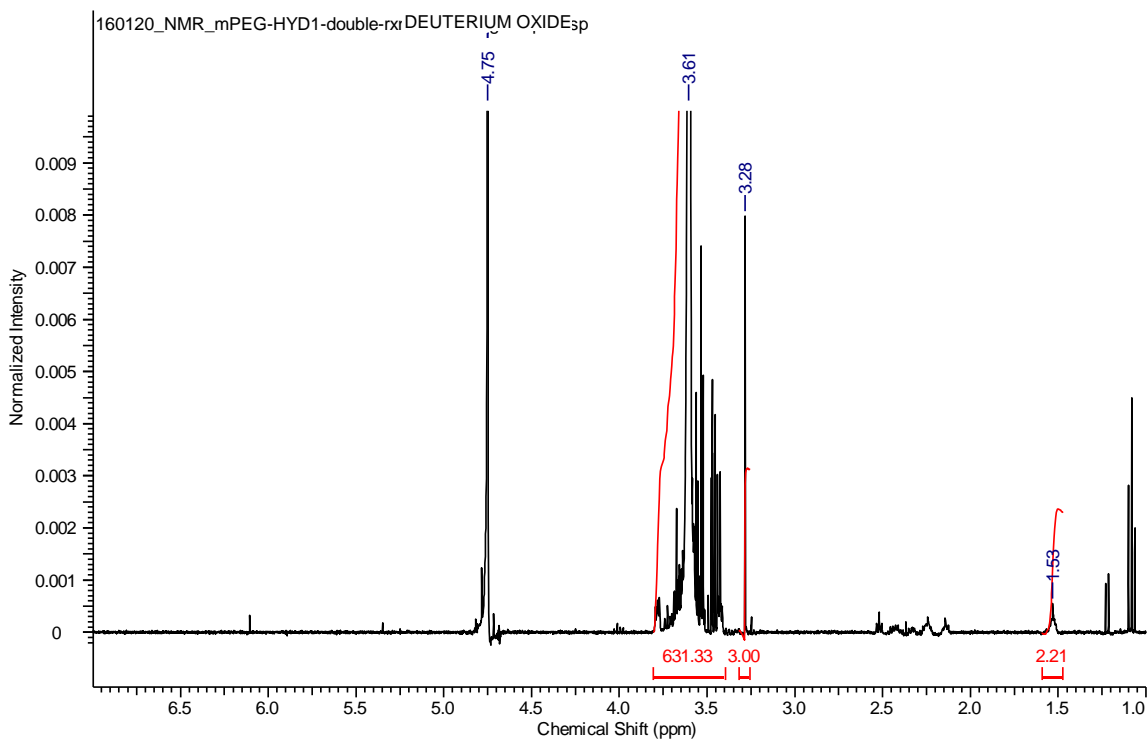


Figure 4.4. NMR Spectrum of mPEG-HYD1 (Twice Reaction with AADH) in D₂O

The result indicated that M_n of the polymer did not change significantly during the hydrazide functionalization reaction and purification steps. Using area of the chemical shifts at 1.56 ppm corresponds to 4 protons, hydrazide conjugation percentage was estimated nearly 54%. In order to test the reproducibility of the reaction, the synthesis was repeated. From ^1H NMR spectrum of this new sample, hydrazide conjugation % was estimated as 53% indicating the reproducibility of the protocol applied. Comparing the COOH functionality of mPEG-propionic acid (80-90%), it was apparent that not all COOH groups were replaced with hydrazide group. For this reason, the polymer with nearly 54% hydrazide functional group was allowed to react one more time with AADH at the same reaction conditions. However, no significant change in hydrazide conjugation percentage was observed as it can be seen in Figure 4.4. Additionally, as a result of the removal of small PEG molecules during dialysis, molar mass of the polymer increased to 6900 Da. Thus, it was concluded that the second functionalization reaction was unnecessary. The same reaction conditions were applied to the synthesis of mPEG-HYD2, since it was not possible to monitor functionalization reaction by NMR when carbohydrazide was used.

4.2. Preparation of PEG-Peptide Based DDS

4.2.1. Peptide (AT1) Synthesis

The *de novo* peptide, AT1, was designed to exploit both ionization properties and reactive functional groups of the amino acid side chains. The peptide sequence given in Figure 3.5 contains basically C, G, H, and E residuals with the following assignments. At the N-terminus of the peptide, C with thiol functional group served as a PEG conjugation site. Histidines (H) were incorporated to provide pH responsiveness to the peptide due to its pK_a value that was around 6.0 as explained in Chapter 2. At the C-terminus, glutamic acid (E) having COO^- group was used to attach DOX. Glycine (G) which is the smallest amino acid with a hydrogen atom in its side chain was placed nearby C and E to minimize steric effects during conjugation.

Purity of AT1 peptide was assessed by ESI-MS and HPLC data is given in Figure 4.5 and Figure 4.6 (a) respectively. In the mass spectrum, theoretical molar mass (1414 Da) of the peptide was confirmed by the peaks corresponding to single and multiple charged peptide m/z values.

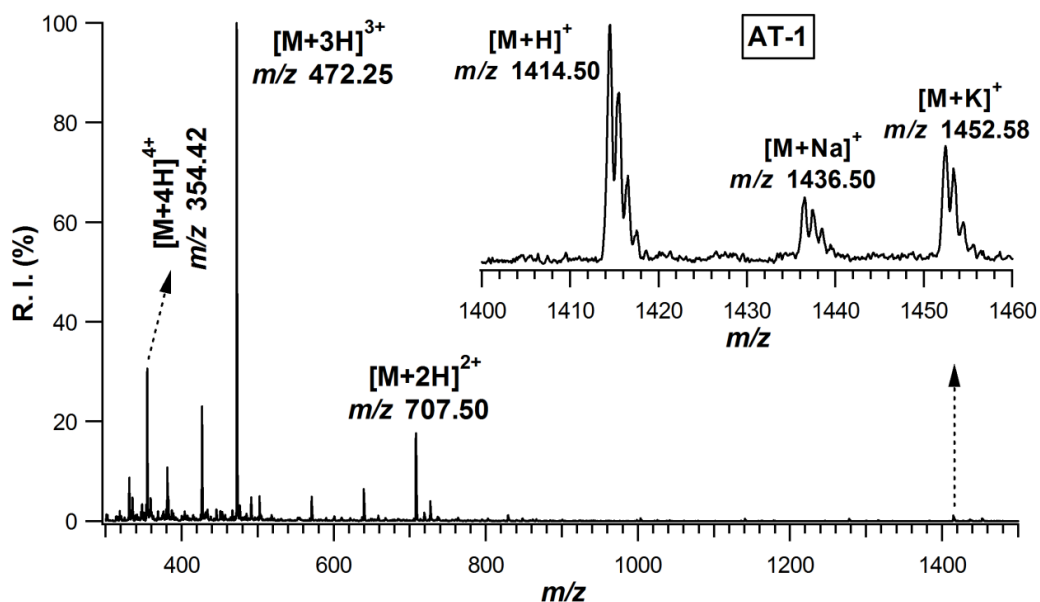


Figure 4.5. ESI-MS Spectrum of AT1 Peptide

HPLC elution curve of the peptide presented a large peak around 24.9 min with relatively small peaks just next to this major peak (Figure 4.6a). The presence of

this highly pure fraction in the HPLC curve along with the consistency of theoretical and experimental molar mass value of the peptide obtained from mass spectrum clearly indicated the peptide was synthesized at high purity.

4.2.2. PEG-Peptide Conjugation

PEGylation of the peptide was carried out using Michael addition reaction between the thiol groups of cysteine located at the N-terminus of the peptide and maleimide form of mPEG ($M_n = 5000$ Da) as given in Figure 3.5. Purity of the isolated mPEG-AT1 conjugate was evaluated by HPLC and MALDI-MS. Figure 4.6 indicates the individual chromatograms of the peptide, mPEG-AT1 and mPEG-maleimide eluted in 24.9, 32.0 and 36.3 min in the order of increasing hydrophobicity. In the elution curve of mPEG-AT1, no significant fractions corresponding to peptide or parent PEG molecule suggesting mPEG-AT1 conjugate have high purity (> 95 %).

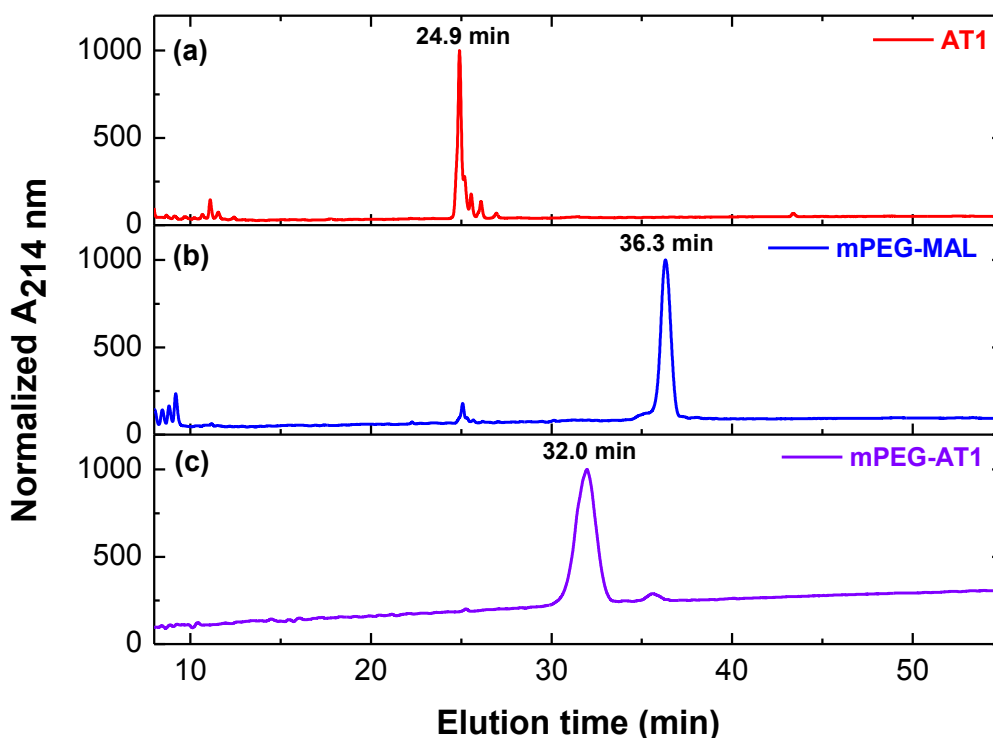


Figure 4.6. HPLC Curves of AT1, mPEG-MAL, and mPEG-AT1

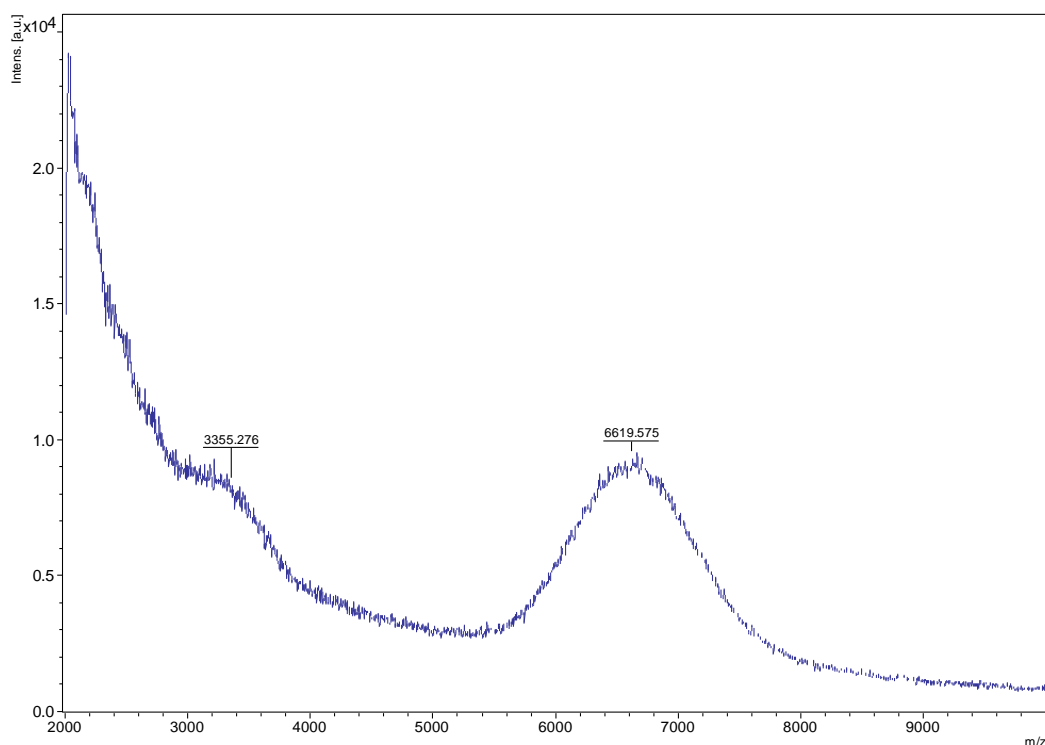


Figure 4.7. MALDI-TOF Spectrum of mPEG-AT1

MALDI-TOF analysis was conducted to determine molecular mass of conjugate. In the mass spectrum of the conjugate a peak was observed at ~6600 Da (Figure 4.7). This experimentally observed molar mass was close to theoretical mass ~6415 Da ($M_{\text{peptide}}=1415$ Da and $M_{\text{PEG}}=5000$ Da) confirming that the conjugation reaction was successful.

Further evidence of the PEGylation of the peptide was also presented by FTIR spectroscopy by comparing the fingerprints of the peptide, mPEG-maleimide, and the conjugate as given in Figure 4.8. It was quite clear that the conjugate had FTIR pattern matching to both parent molecules. More specifically, the band around 2900 cm^{-1} assigned to C-H stretching of PEG backbone appeared in the FTIR spectra of both PEG and the conjugate. Similarly, amide I and amide II bands of peptide observed in $1500\text{--}1700\text{ cm}^{-1}$ region were obvious in the spectrum of the conjugate. Thus, the three characterization method confirmed that high purity of mPEG-peptide conjugate was isolated.

In the next step of the synthesis of PEG-peptide based DDS, mPEG-AT1 was functionalized with AADH to create acid cleavable DOX attachment site (Figure 3.6).

Unfortunately, it was not possible to determine hydrazide functionality % of the DDS due to the complex form of the NMR spectrum with possible overlapped chemical shifts.

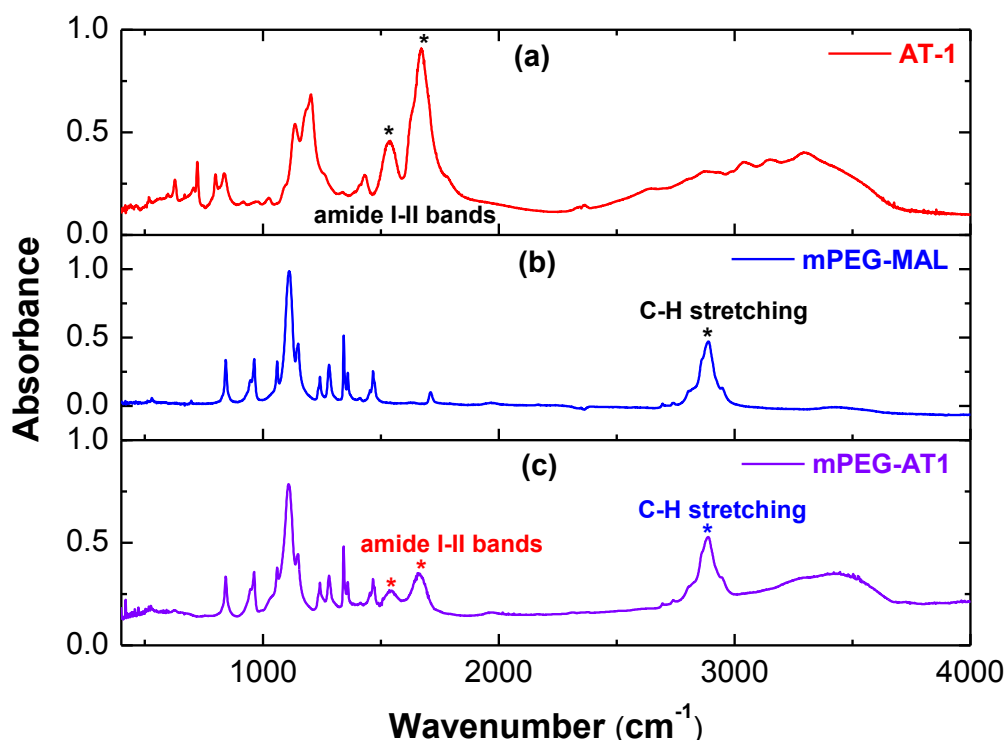


Figure 4.8. FTIR Spectra of (a) AT1, (b) mPEG-MAL, and (c) mPEG-AT1

4.3. DOX Conjugation to PEG and PEG-Peptide Based DDS

After ensuring reproducible hydrazide conjugation as described in Section 4.1, in the following step, a few reaction conditions were tested to achieve maximum DOX functionalization. For this purpose, catalyst (TFA acid), DOX amount and addition procedure were changed (Table 4.1) and DOX conjugation % was determined using UV-Vis spectroscopy based on the extinction coefficient of free DOX at 488 nm. UV-Vis Spectra of the DOX conjugated samples are given in Figure A.7 in Appendix A. Table 4.1 indicated that highest DOX conjugation % was achieved using 2% catalyst, with HYD: DOX ratio of 2.5:2 by mass and by the single addition method (third route).

Table 4.1. Optimization of DOX Functionalization

Sample Code	HYD1 : DOX Ratio	DOX Addition Method	TFA Amount (μ l)	DOX % Functional Group	Product Yield % *
S1	2.5:1	Single Addition	10	41	33.8
S2	2.5:1	Single Addition	20	45	46
S3	2.5:2	Single Addition	20	63	35
S4	2.5:2	Double Addition	20	56	39

*Product Yield: Ratio of product amount to initial amount of mPEG-HYD1

In some reaction conditions DOX conjugation percentage was obtained as ~56-63%, slightly higher than hydrazide functionalization (~54 %). This can be attributed to either remaining free DOX in the conjugates that could not be separated during GPC or the imprecise measurement of DOX amount in the conjugates. In the purification of the conjugates, a clear color difference was apparent in the elution fractions of GPC (conjugates = red, free DOX = orange) suggesting most of the free DOX was separated (Figure A.8). Therefore, the difference between the values of extinction coefficient of free DOX and conjugated DOX was likely to be the reason for the overestimation of the DOX conjugation % values. However, in the absence of other techniques such as HPLC which required much higher concentration, UV estimation of conjugated drug content has been employed due to its simplicity and much lower sample requirement.

DOX conjugation of PEG and PEG-peptide based drug delivery systems were carried out using the third route explored above at large scale. The properties of the DDS developed are shown in Table 4.2.

Table 4.2. PEG and PEG-Peptide Based DDS Used for DOX Conjugation

Sample	Components	Theoretical MW (Da)	Property
mPEG-HYD1	mPEG-adipic acid hydrazide	~ 5000	Acid cleavable bond
mPEG-HYD2	mPEG-carbohydrazide	~ 5000	Acid cleavable bond
mPEG-AT1-HYD	mPEG-CGGGHHHHHHGGGE-adipic acid hydrazide	6414.5	Acid cleavable bond + pH responsive

Table 4.3. DOX Conjugation Yields and % of the DDS

Sample Code	Yield %	DOX Conjugation %
mPEG-HYD1-DOX	65 ± 3	62 ± 7
mPEG-HYD2-DOX	68 ± 3	60 ± 3
mPEG-AT1-DOX	43 ± 3	35 ± 3

DOX conjugation reaction results are given in Table 4.3. The conjugation reactions of the DDS at large scale seem reproducible with reasonable standard deviation values of yield and DOX conjugation %. More specifically, for mPEG-HYD1, DOX conjugation % was consistent at both small scale and large scale. The yield at large scale was higher as expected. DOX conjugation % of PEG based DDS (~ 60%) was found to be higher than that of the PEG-peptide based DDS. The possible reason can be increased steric hindrance effect of the more crowded environment nearby drug conjugation site in the case of PEG-peptide DDS.

4.4. Characterization of DOX Conjugated Drug Delivery Systems

4.4.1. Size Measurement

Dynamic light scattering was used to determine aggregation state and stability of the DOX conjugated DDS. Figure 4.9 shows size (hydrodynamic diameter) distribution of mPEG-propionic acid, mPEG-HYD1, and mPEG-HYD2 in PBS buffer (pH 7.4) and mPEG-AT1 in both PBS and acetate buffer (pH 5.0). Average size of the samples was determined to be similar for all the samples with a value around $\sim 4 \pm 0.5$ nm. It was also observed that pH change did not affect the size of mPEG-AT1.

It is possible to predict hydrodynamic diameter (D_H) of PEG as a function of its molar mass (M_n) via the following correlation (Fee et al., 2006):

$$D_H (\text{\AA}) = 0.3824 M_n^{0.559} \quad (4.1)$$

The use of the equation above gave size of a PEG molecule with a molar mass of 5000 Da as ~ 4.4 nm, which was consistent with the experimental values. Thus, it can

be concluded that neither functionalized PEGs nor PEG-AT1 conjugate had aggregation tendency.

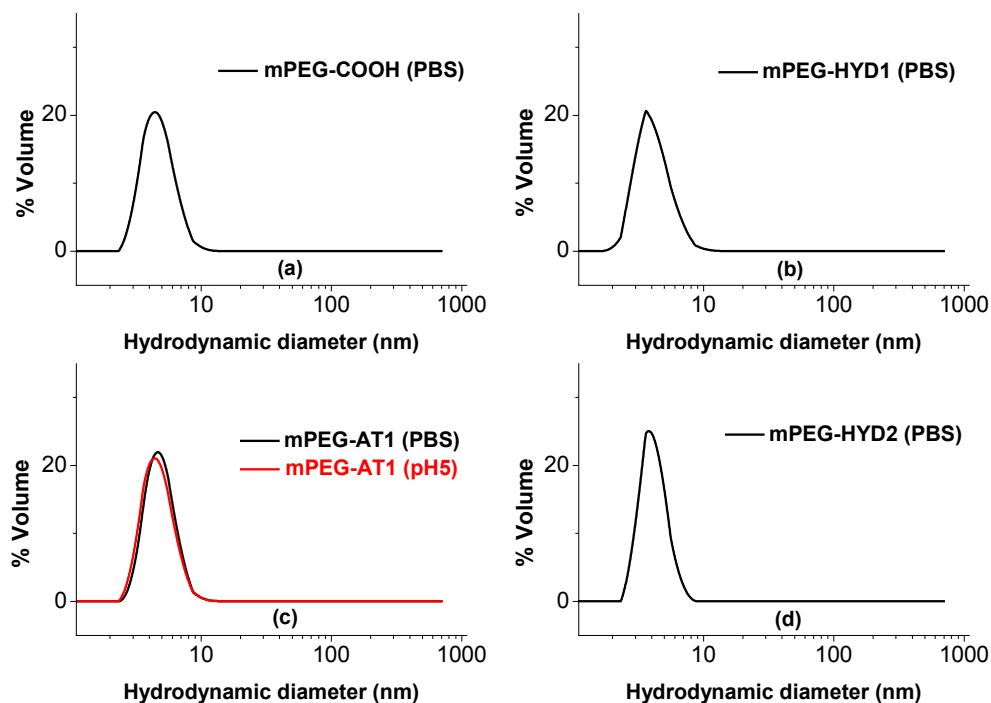


Figure 4.9. Size Distribution of PEGs with Different Functional Groups and PEG-AT1 Conjugate

Size distributions of the DOX-conjugated DDS followed completely different patterns. The measurements were taken within a few hours after the dissolution of the conjugates in appropriate buffer and after incubating the solution at 37°C for 1 day. The resultant curves are given in Figure 4.10 and Figure 4.11 for the immediate measurement and following 24hr incubation period, respectively. Average sizes of mPEG-HYD1-DOX at pH 7.4 and pH 5.0 upon immediate measurement were obtained as 9 ± 0.5 nm and 7 ± 0.5 nm respectively. After 24hr incubation, size values at both pH reduced to 6.5 ± 0.5 nm. The average size of the conjugate at pH 7.4 was about twice of mPEG-HYD1 molecule. Thus, it can be suggested that drug conjugation to the carrier molecule, mPEG-HYD1, triggered self-assembly of the DOX conjugated DDS resulting micellar aggregates in which drug molecules were in the core and PEG molecules were at the surface. Approximately, 1-2 nm reduction in the average size of mPEG-HYD1-

DOX was observed at pH 5 and after 24 hours incubation period. It was likely due to the increase in the population of monomeric (non-aggregated) species upon the departure of the drug molecules from the micellar structures.

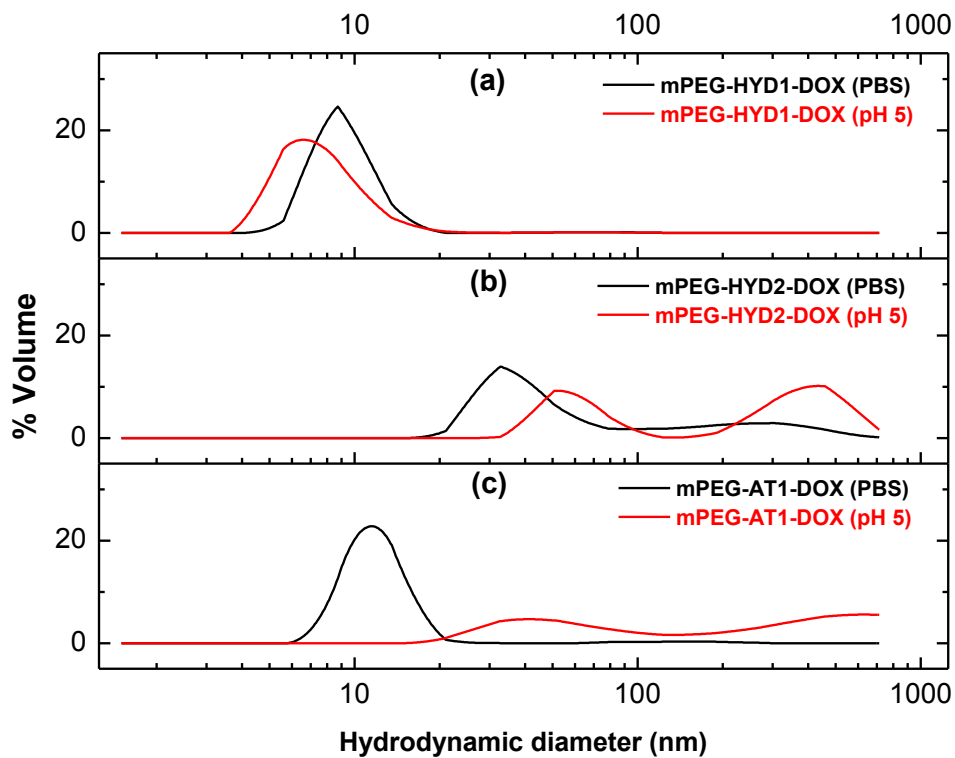


Figure 4.10. Size Distributions of the As Prepared DOX-Conjugated DDS

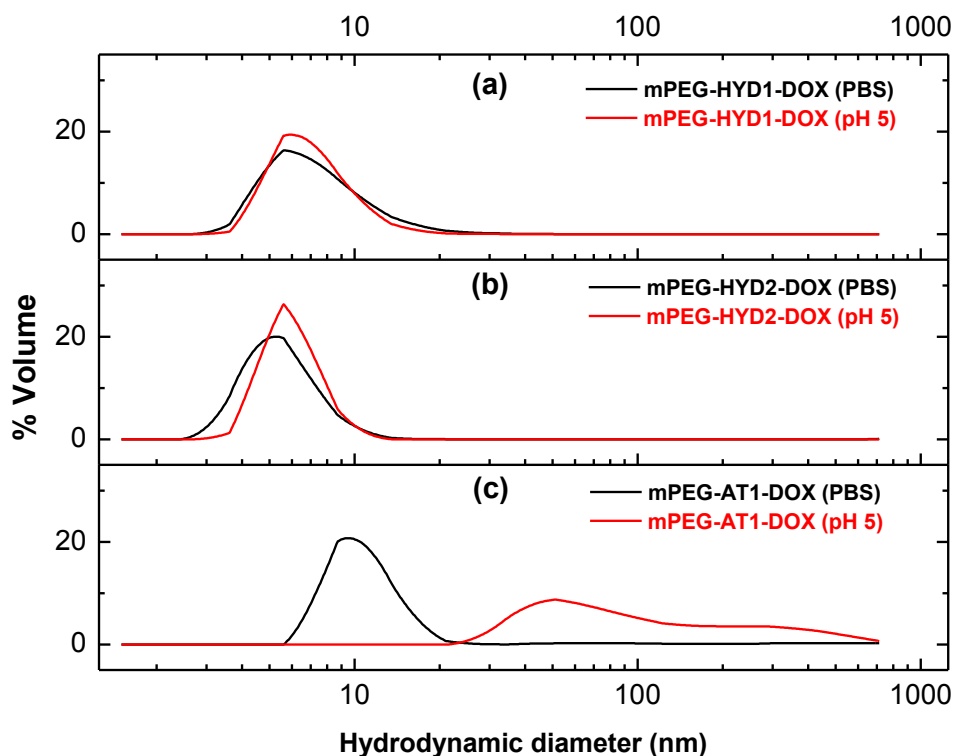


Figure 4.11. Size Distributions of the DOX-Conjugated DDS Obtained After 24 hrs Incubation

The other PEG based DDS, mPEG-HYD2-DOX presented size distribution between ~ 20 - 100 nm initially independent of pH. Upon incubation for prolonged time, the size of the aggregates shrunk to $\sim 6 \pm 1$ nm for both pH cases. One of the speculations that most likely explained the reduction in the size can be instability of the chemical bond causing the immediate release of drug followed by the rearrangement of the aggregates with time. It was possible that sudden release of drug may cause the aggregation of large number of drug molecules requiring more PEG molecules to stabilize them. The aggregate system can be visualized as a core shell micellar system suggested for mPEG-HYD1-DOX but not essentially spherical and having a larger core surrounded by PEG molecules attached mostly physically to surface of the drugs. Upon incubation at higher temperature, the increased mobility of the molecules may have caused rearrangement of the aggregate structures via the decomposition of an intact large aggregate into a number of smaller aggregates.

mPEG-peptide based DDS, mPEG-AT1-DOX, have similar type of chemical bond between the carrier and drug molecule as in mPEG-HYD1. However, different

from this PEG (only)-based DDS, mPEG-AT1-DOX also contained pH responsive peptide domain. Therefore, the role of the peptide domain in the DOX-conjugated DDS can be elucidated by comparing its size distribution data with those of mPEG-HYD1-DOX. At pH 7.4, slightly larger average size ($\sim 12 \pm 2$ nm) was obtained for mPEG-AT1-DOX due to the addition of the peptide block. No significant change in the size observed upon incubation at 37°C for a day, similar to the behavior of mPEG-HYD1-DOX. Considering the size of the aggregates was slightly higher than twice of the parent molecule, mPEG-AT1, it can be deduced that shape of the aggregates was likely to be slightly deviating from spherical arrangement. At pH 5, on the other hand, larger aggregate sizes ranging from 20 to 100 nm were obtained for mPEG-AT1-DOX. This distribution was similar to that of mPEG-HYD2-DOX but the aggregates of mPEG-AT1-DOX were more stable as indicated by no significant change in size distribution after the incubation period. In one scenario, the repulsions between positively charged histidines at pH 5.0 may prevent close spherical packing of the molecules but drive the molecules to form loosely packed elongated structures with size larger than spherical aggregates. Alternative explanation can be similar to the one proposed in the case of mPEG-HYD2-DOX. Although both had the similar chemical bonds, different from mPEG-HYD1-DOX, charged peptide domain may have destabilized or prevented the formation of tight packing of the aggregates, by allowing solvent to access the pH cleavable bond and hence increasing the release rate of the drug in the case of mPEG-AT1-DOX. It is possible that faster release of drug molecules may be resulted in larger size of drug aggregates that needs to be stabilized by larger number of hydrophilic carrier molecules than those required for spherical aggregates. Surprisingly, in contrast to mPEG-HYD2-DOX, these large aggregates were observed to be more stable requiring strong interactions between peptide block and drug molecules by preventing structural rearrangement of the aggregates. In this second scenario, free drug concentration in solvent phase was expected to be lower compared to the first scenario.

4.4.2. Drug Release Profiles

DOX release profiles of mPEG-HYD1-DOX, mPEG-HYD2-DOX and mPEG-AT1-DOX at pH 7.4 and pH 5.0 are given in Figure 4.12, 4.13, and 4.14 respectively. DOX release % values of each DDS at the end of 72 hours period are

summarized in Table 4.4 along with the drug release properties of other DDS containing acid cleavable hydrazone bond. These results indicated that mPEG-HYD1-DOX had slight pH responsive drug release behavior. No significant difference was observed in the release profiles of mPEG-HYD2-DOX at acidic and neutral pH. On the contrary, PEG-peptide based DDS, mPEG-AT1-DOX presented faster DOX release with more pronounced pH programmed release behavior compared to PEG-only DDS.

Comparison of the other DDS suggested that the release behavior of mPEG-HYD1 was similar to mPEG-PLLA-HYD-DOX system where single DOX was attached to the carrier amphiphilic molecule which had inherent tendency to form compact aggregates (Yoo et al., 2002). pH responsiveness was observed to be more apparent multivalent mPEG-polyaspartate-HYD-DOX and can be attributed to more compact aggregates as revealed by no release at all at neutral pH (Bae et al., 2003). In the systems having no aggregation tendency as in PEO-g-HYD-DOX, DOX release rate was found to be much higher than that of aggregated DDS (Zhou et al., 2011). When the sizes of designed DOX-conjugated DDS were compared, mPEG-AT1-DOX would seem least likely to present the highest DOX release ability. However, it is supposedly the charged peptide block in mPEG-AT1-DOX that loose the interactions between the aggregated molecules thereby facilitating the contact of the solvent molecules with the pH responsive hydrazone bonds. As revealed by the size of the mPEG-AT1-DOX, the number of charged histidines in the peptide was not enough to completely destabilize the aggregates. Thus, it can be speculated that incorporation of more histidines to the peptide block of the carrier molecule can be resulted in faster DOX release with higher pH sensitivity.

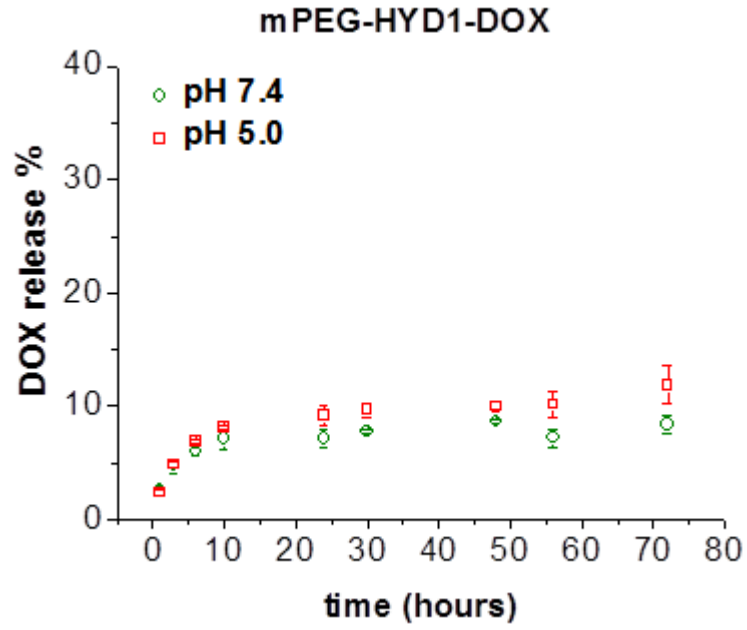


Figure 4.12. mPEG-HYD1-DOX Drug Release Curves at pH 5.0 and 7.4

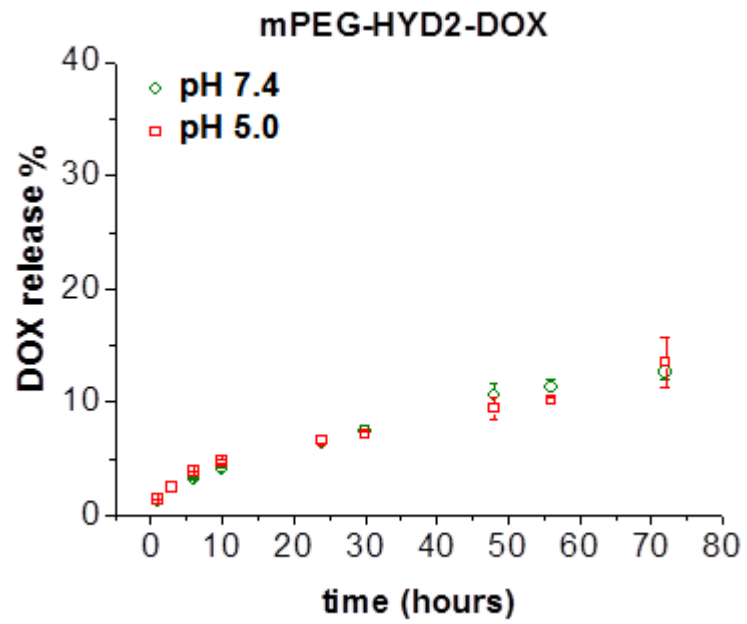


Figure 4.13. mPEG-HYD2-DOX Drug Release Curves at pH 5.0 and 7.4

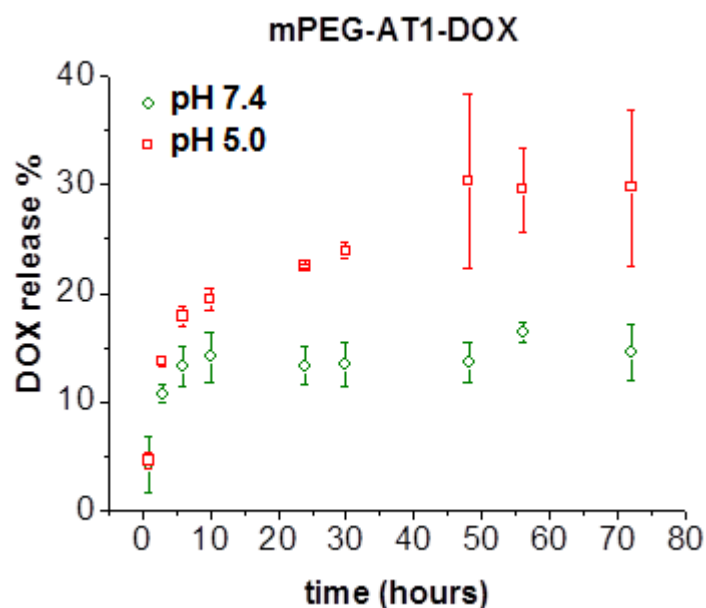


Figure 4.14. mPEG-AT1-DOX Drug Release at pH 5.0 and 7.4

Table 4.4. Comparison of Drug Release % Values of Various DDS at Neutral and Acidic pH

Reference	DDS	Size (nm)	% DOX release at pH 5.0	% DOX release at pH 7-7.5
Current study	mPEG-HYD1-DOX	9	12 ± 2	8 ± 1
Current study	mPEG-HYD2-DOX	20-100	13.5 ± 2.5	12.5 ± 0.5
Current study	mPEG-AT1-DOX	12	30 ± 7	14.5 ± 2.5
Bae et al. 2003	mPEG-polyaspartate-HYD-DOX	65	28	0
Zhou et al. 2011	PEO-g-HYD-DOX	9-11	90	20
Yoo et al. 2002	mPEG-PLLA-HYD-DOX*	90 ± 12	24	20

* Drug release % was recorded at the end of 25 hrs. For the other DDS, the values correspond to the end of 72 hrs period.

4.4.3. Cytotoxicity

Cytotoxicity of the samples was determined by measuring viability of lung cancer cells (A-549) grown over RPMI medium via MTT assay. MTT test was conducted at different number of cells (5000, 7500, and 10000 cells/well) to select the

optimal cell number giving absorbance readings between 0.75-1.25. As indicated in Figure A.9, 5000 cells/well was found appropriate for the cytotoxicity tests.

Cytotoxicity results of mPEG-propionic acid, AADH, mPEG-HYD1 and AT1 peptide at 1.5 mg/ml concentration are given in Figure 4.15. No significant toxicity of these samples was revealed. Growth curve assay results of free DOX and the DOX conjugated DDS are given in Figure 4.16. The resultant IC₅₀ values are summarized in Table 4.5. For free DOX.HCl, viability % started to increase at concentrations higher than ~0.5 µg/ml. In the MTT protocols applied earlier where MTT was directly contacted with DOX.HCl, the absorbance value was observed to increase with increasing DOX concentration. When the drug solution was discarded before applying MTT solution as in the current protocol, this effect was minimized but the remaining DOX molecules were found to interfere absorbance value at high concentrations. For this reason, initial portion of the growth inhibition curve of DOX was considered in the determination of its IC₅₀ value. DOX-conjugated DDS exhibited higher IC₅₀ value than free DOX as expected. Of these conjugates, mPEG-AT1-DOX presented higher toxicity. Considering no significant toxicity of AT1, the superior cytotoxicity of PEG-AT1-DOX was due to its pronounced pH responsive behavior.

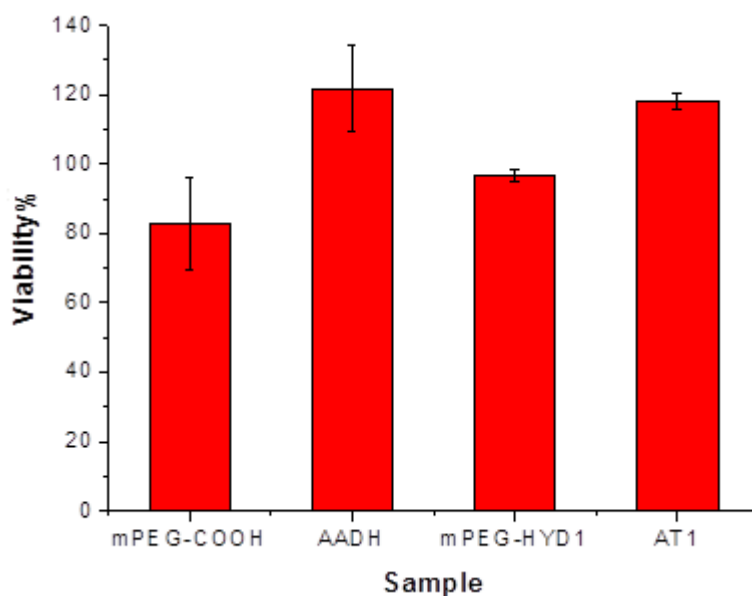


Figure 4.15. Cytotoxicity of mPEG-COOH, AADH, mPEG-HYD1, and AT1

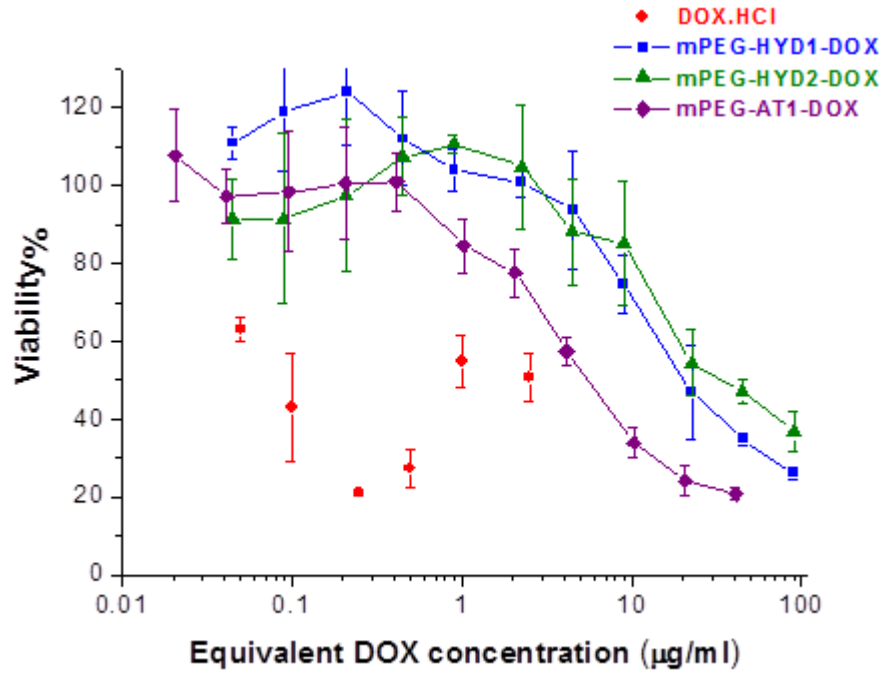


Figure 4.16. Growth Inhibition Curves of Free DOX and DOX-Conjugated DDS

Table 4.5. IC₅₀ Values of the Samples

Sample	DOX equivalent IC ₅₀ value (µg/ml)	Relative index*
DOX	0.07	1.000
mPEG-HYD1-DOX	20	286
mPEG-HYD2-DOX	40	572
mPEG-AT1-DOX	5	70

*Ratio between IC₅₀ values of the DDS and DOX

CHAPTER 5

CONCLUSIONS

In the first part of the study, drug delivery systems composed of mPEG, acid cleavable hydrazone bond and DOX was synthesized. AADH and CH were used to generate DOX attachment site. In the second part, pH responsive peptide mPEG conjugate system was synthesized and DOX was attached hydrazide form of the conjugate prepared using AADH. Approximately 53% hydrazide functionalization was obtained in the reactions between mPEG-carboxylic acid and AADH. Slightly higher DOX conjugation (63%) to hydrazide form of this molecule as determined could be due to either presence of free DOX or inaccuracy of the DOX measurement.

Although peptide containing conjugate (mPEG-AT1-DOX) had lower DOX conjugation (~35%) which can be attributed to steric effects, it exhibited more pronounced pH responsiveness as indicated by the drug release studies performed at pH 5.0 and pH 7.4. Superior drug release properties and cytotoxicity of mPEG-AT1-DOX compared to PEG-DOX conjugate systems suggested the conjugates containing both pH responsive the domains and chemical bonds could be promising drug delivery systems. However, to exploit EPR effect larger size of the DOX-conjugated carrier molecule should be required. Such a system may be possible by the development of a multivalent system where a number of drug molecules can be attached or by decreasing the length of the hydrophilic PEG block. Additionally, pH sensitivity of the DDS can be improved by the incorporation of more histidines to the peptide domain.

REFERENCES

- Akinc, A.; Anderson, D.G.; Lynn, D.M.; Langer, R. Synthesis of Poly(Beta-Amino Ester)s Optimized for Highly Effective Gene Delivery. *Bioconjugate Chemistry*. **2003**, 14(5), 979-988.
- Altan, N.; Chen, Y.; Schindler, M.; Simon, S.M. Defective Acidification in Human Breast Tumor Cells and Implications for Chemotherapy. *Journal of Experimental Medicine*. **1998**, 187(10), 1583-1598.
- Bae, Y.; Fukushima, S.; Harada, A.; Kataoka K. Design of Environment-Sensitive Supramolecular Assemblies for Intracellular Drug Delivery: Polymeric Micelles that are Responsive to Intracellular pH Change. *Angewandte Chemie. International Edition*. **2003**, 42(38), 4640-4643.
- Barnie, P. A.; Zhang, P.; Lu, P.; Chen, X.; Su, Z.; Wang, S.; Xu, H. cPg-Oligodeoxynucleotides Suppress the Proliferation of A549 Lung Adenocarcinoma Cells via Toll-Like Receptor 9 Signaling and Upregulation of Runt-Related Transcription Factor 3 Expression. *Biomedical Reports*. **2014**, 2(3), 374-377.
- Barrett, J. Mechanisms of Multistep Carcinogenesis and Carcinogen Risk Assessment. *Environmental Health Perspectives*. **1993**, 100, 9-20.
- Berenblum, I.; Shubik, P. A New, Quantitative, Approach to the Study of the Stages of Chemical Carcinogenesis in the Mouse's Skin. *British Journal of Cancer*. **1947**, 1(4), 383-391.
- Bernkop-Schnürch, A.; Dünnhaupt, S. Chitosan-Based Drug Delivery Systems. *European Journal of Pharmaceutics and Biopharmaceutics*. **2012**, 81(3), 463-469.
- Blazkova, I.; Nguyen, H.V.; Dostalova, S.; Kopel, P.; Stanisavljevic, M.; Stiborova, M.; Eckschlager, T.; Kizek, R.; Adam, V. Apoferritin Magnetic Particles as Doxorubicin Carriers for Anticancer Drug Delivery. *International Journal of Molecular Sciences*. **2013**, 14(7), 13391-13402.

- Boyd, J.A.; Barrett, J.C. Genetic and Cellular Basis of Multistep Carcinogenesis. *Pharmacology & Therapeutics*. **1990**, 46(3), 469-486.
- Boyle P.; Levin, B. *World Cancer Report*; International Agency for Research on Cancer: World Health Organization, **2008**.
- Chaffee, S.; Mary, A.; Stiehm, E.R.; Girault, D.; Fischer, A.; Hershfield, M.S. IgG Antibody Response to Polyethylene Glycol-Modified Adenosine Deaminase in Patients with Adenosine Deaminase Deficiency. *Journal of Clinical Investigation*. **1992**, 89(5), 1643-1651.
- Cheng, T.; Chuang, K.; Chen, B.; Roffler, S.R. Analytical Measurement of PEGylated Molecules. *Bioconjugate Chemistry American Chemical Society*. **2012**, 23(5), 881-899.
- Cheng, T.L.; Chen, B.M.; Chan, L.Y.; Wu, P.Y.; Chern, J.W.; Roffler, S.R. Poly(ethylene glycol) Modification of Beta-Glucuronidase-Antibody Conjuates for Solid-Tumor Therapy by Targeted Activation of Glucuronide Prodrugs. *Cancer Immunology, Immunotherapy*. **1997**, 44(6), 305-315.
- Cole, S.P.C.; Bhardwaj, G.; Gerlach, J.H.; Mackie, J.E.; Grant, C.E.; Almquist, K.C. Overexpression of a Transporter Gene in a Multidrug-Resistant Human Lung Cancer Cell Line. *Science*. **1992**, 258(5088), 1650-1654.
- Conde, J.; Ambrosone, A.; Sanz, V.; Hernandez, Y.; Marchesano, V.; Tian, F.; Child, H.; Berry, C.C.; Ibarra, M.R.; Baptista, P.V.; Tortiglione, C.; Fuente, J.M. Design of Multifunctional Gold Nanoparticles for in vitro and in vivo Gene Silencing. *American Chemical Society Nano*. **2012**, 6(9), 8316-8324.
- Conde, J.; Dias, J.T.; Grazu, V.; Moros, M.; Baptista, P.V.; Fuente, J.M. Revisiting 30 Years of Biofunctionalization and Surface Chemistry of Inorganic Nanoparticles for Nanomedicine. *Frontiers in Chemistry*. **2014**, 2, 1-27.
- Configliacchi, E.; Razzano, G.; Rizzo, V.; Vigevani, A. HPLC Methods for the Determination of Bound and Free Doxorubicin, and of Bound and Free Galactosamine, in Methacrylamide Polymer-Drug Conjugates. *Journal of Pharmaceutical and Biomedical Analysis*. **1996**, 15(1), 123-129.

- Cox, R. Mechanisms of Radiation Oncogenesis. *International Journal of Radiation Biology*. **1994**, 65(1), 57-64.
- Darr, A.; Calabro, A. Synthesis and Characterization of Tyramine Based Hyaluronan Hydrogels. *Journal of Materials Science: Materials in Medicine*. **2009**, 20(1), 33-44.
- Engin, K.; Leeper, D.B.; Cater, J.R.; Thistlethwaite, A.J.; Tupchong, L.; McFarlane, J.D. Extracellular pH Distribution in Human Tumors. *International Journal of Hyperthermia*. **1995**, 11(2), 211-216.
- Etrych, T.; Jelinkova, M.; Rihova, B.; Ulbrich, K. New HPMA Copolymers Containing Doxorubicin Bound via pH-Sensitive Linkage: Synthesis and Preliminary in Vitro and in Vivo Biological Properties. *Journal of Controlled Release*. **2001**, 73(1), 89-102.
- Fang, J.; Nakamura, H.; Iyer, A.K. Tumor-Targeted Induction of Oxystress for Cancer Therapy. *Journal of Drug Targeting*. **2007**, 15(7-8), 475-486.
- Farokhzad, O. C.; Langer, R. Nanomedicine: Developing Smarter Therapeutic and Diagnostic Modalities. *Advanced Drug Delivery Reviews*. **2006**, 58(14), 1456–1459.
- Fee, C.J.; Van Alstine, J.M. PEG-Proteins: Reaction Engineering and Separation Issues. *Chemical Engineering Science*. **2006**, 61(3), 924-939.
- Fidler, I.J.; Kim, S.J. The Role of the Organ Microenvironment in the Biology and Therapy of Cancer Metastasis. *Journal of Cellular Biochemistry*. **2007**, 101(4), 927-936.
- Fishel, R.; Kolodner R.D. The Identification of Mismatch Repair Genes and Their Role in the Development of Cancer. *Current Opinion in Genetics & Development*. **1995**, 5(3), 382-395.
- Florence, A.T.; Salole, E.G. Pharmaceutical Aspects of Cancer Chemotherapy. *Topics in Pharmacy*; Florence, A.T.; Salole, E.G. Elsevier, 1993; Vol. 3.

- Ghasemi, S.; Davarani, S.; Sharif, S.; Asgari, D.; Abdollahi, A.; Mojarrad, J.S. Comparison of Cytotoxic Activity of L778123 as a Farnesyltransferase Inhibitor and Doxorubicin Against A549 and HT-29 Cell Lines. *Advanced Pharmaceutical Bulletin*. **2013**, 3(1), 73-77.
- Gillies, E.R.; Frechet, J.M.J. pH-Responsive Copolymer Assemblies for Controlled Release of Doxorubicin. *Bioconjugate Chemistry*. **2005**, 16(2), 361-368.
- Gillies, E. R.; Frechet, J. M. J. Development of Acid Sensitive Copolymer Micelles for Drug Delivery. *Pure and Applied Chemistry*. **2004**, 76, 1295-1307.
- Gong, X.W.; Wei, D.Z.; He, M.L. & Xiong, Y.C. Discard Free PEG-Based Assay for Obtaining the Modification Extent of PEGylated Proteins. *Talanta*. **2007**, 71(1), 381-384.
- Haag, R. Supramolecular Drug-Delivery Systems Based on Polymeric Core-Shell Architectures. *Angewandte Chemie International Edition*. **2003**, 43(3), 278-282.
- Harris, J.M.; Chess, R.B. Effect of Pegylation on Pharmaceuticals. *Nature Reviews Drug Discovery*. **2003**, 2(3), 214-221.
- Hartwell, L.H.; Kastan, M.B. Cell Cycle Control and Cancer. *Science*. **1994**, 266(5192), 1821-1828.
- He, H.; Zhao, J.; Jia, R.; Zhao, Y.; Yang, S.; Yu, L.; Yang, L. Novel Pyrazolo [3,4-d] Pyrimidine Derivative as Potential Antitumor Agents: Exploratory Synthesis, Preliminary Structure-Activity Relationships and in Vitro Biological Evaluation. *Molecules*. **2011**, 16(12), 10685-10694.
- Heffernan, M.J.; Murthy, N. Polyketal Nanoparticles: A New pH-Sensitive Biodegradable Drug Delivery Vehicle. *Bioconjugate Chemistry*. **2005**, 16(6), 1340-1342
- Hermanson, G. H. *Bioconjugate Techniques*; American Chemical Society: San Diego, 1997; Vol. 40. Academic Press, San Diego

- Hoare, D.G.; Koshland, D.E. A Method for the Quantitative Modification and Estimation of Carboxylic Acid Groups in Proteins. *Journal of Biological Chemistry*. **1967**, 242, 2447-2453.
- Janssen, M.; Mihov, G.; Welting, T.; Thies, J. Emans P. Drugs and Polymers for Delivery Systems in OA Joints: Clinical Needs and Opportunities. *Polymers*. **2014**, 6(3), 799-819.
- Kamaly, N.; Kalber, T.; Thanou, M.; Bell, J.D.; Miller, A.D. Folate Receptor Targeted Bimodal Liposomes for Tumor Magnetic Resonance Imaging. *Bioconjugate Chemistry*. **2009**, 20(4), 648-655.
- Keating, M.J.; Holmes, R.; Lerner, S.; Ho, D.H. L-asparaginase and PEG Asparaginase-Past, Present and Future. *Leukemia & Lymphoma*. **1993**, 10, 153-157.
- Kim, G.M.; Bae, Y.H.; Jo, W.H. pH-Induced Micelle Formation of Poly(Histidine-co-Phenylalanine)-Block-Poly(Ethyleneglycol) in Aqueous Media. *Macromolecular Bioscience*. **2005**, 5(11), 1118-1124.
- Kim., J.H.; Kim, Y.S.; Park, K.; Kang, E.; Lee, S.; Nam, H.Y.; Kim, K.; Park, J.H; Chi, D.Y.; Park, R.W.; Kim, I.S.; Choi, K.; Kwon, I.C. Self- Assembled Glycol Chitosan Nanoparticles for the Sustained and Prolonged Delivery of Antiangiogenic Small Peptide Drugs in Cancer Therapy. *Biomaterials*. **2008**, 29(12), 1920-1930.
- Kwon, G.S.; Okano, T. Polymeric Micelles as New Drug Carriers. *Advanced Drug Delivery Reviews*. **1996**, 21(2), 107-116.
- Land, H.; Parada, L.F.; Weinberg, R.A. Cellular Oncogenes and Multi-Step Carcinogenesis. *Science*. **1983**, 222(4625), 771-778.
- Lee, E. S.; Na, K.; Bae, Y.H. Polymeric Micelle for Tumor pH and Folate-Mediated Targeting. *Journal of Controlled Release*. **2003**, 91(1-2), 103-113.

- Lee, E.S.; Oh, K.T.; Kim, D.; Youn, Y.S.; Bae, Y.H. Tumor pH-Responsive Flower-Like Micelles of Poly(L-Lactic Acid)-b-Poly(Ethylene Glycol)-b-Poly(L-Histidine). *Journal of Controlled Release*. **2007**, 123(1), 19-26.
- Lee, E.S.; Shin, H.J.; Na, K.; Bae, Y.H. Poly(L-Histidine)-PEG Block Copolymer Micelles and pH-Induced Destabilization. *Journal of Controlled Release*. **2003**, 90(3), 363-374.
- Lynn, D.M.; Amiji, M.M.; Langer, R. pH Responsive Polymer Microspheres: Rapid Release of Encapsulated Material within the Range of Intracellular pH. *Angewandte Chemie International Edition*. **2001**, 40(9), 1707-1710.
- Lynn, D.M.; Anderson, D.G.; Putnam, D.; Langer, R. Accelerated Discovery of Synthetic Transfection Vectors: Parallel Synthesis and Screening of a Degradable Polymer Library. *Journal of the American Chemical Society*. **2001**, 123(33), 8155-8156.
- Ma Y.; Fan X.; Li L. pH-Sensitive Polymeric Micelles Formed by Doxorubicin Conjugated Prodrugs for Co-Delivery of Doxorubicin and Paclitaxel. *Carbohydrate Polymers*. **2016**, 137, 19-29.
- Maeda, H.; Matsumura, Y. Tumoritropic and Lymphotropic Principles of Macromolecular Drugs. *Critical Reviews in Therapeutic Drug Carrier Systems*. **1989**, 6(3), 193-210.
- Maeda, H.; Wu, J.; Sawa, T.; Matsumura, Y.; Hori, K. Tumor Vascular Permeability and the EPR Effect in Macromolecular Therapeutics: A Review. *Journal of Controlled Release*. **2000**, 65(1-2), 271-284.
- Mero, A.; Schiavon, O.; Pasut, G.; Veronese, F.M. A Biodegradable Polymeric Carrier Based on PEG for Drug Delivery. *Journal of Bioactive and Compatible Polymers*. **2009**, 24, 220-234.
- Gottesman, M.M.; Pastan, I. Biochemistry of Multidrug Resistance Mediated by the Multidrug Transporter. *Annual Review of Biochemistry*. **1993**, 62, 385-427.

- Minh, H.P.T.; Phuong, L.L.; Van, L.N.; Thanh, H.N.; Anh, S.H.; Linh, T.N.; Thanh, T.B. Developing and Evaluating in Vitro Effect of PEGylated Liposomal Doxorubicin on Cancer Cells. *Journal of Chemical and Pharmaceutical Research*. **2015**, 7(3), 2239-2243.
- Nakajima, N.; Ikada, Y. Mechanism of Amide Formation by Carbodiimide for Bioconjugation in Aqueous Media. *Bioconjugate Chemistry*. **1995**, 6(1), 123-130.
- Nogueira, D.R.; Mitjans, M.; Infante, M.R.; Vinardell, M.P. Comparative Sensitivity of Tumor and Non-Tumor Cell Lines As a Reliable Approach for in Vitro Cytotoxicity Screening of Lysine-Based Surfactants with Potential Pharmaceutical Applications. *International Journal of Pharmaceutics*. **2011**, 420, 51-58.
- Noonan, K.E.; Beck, C.; Holzmayer, T.A.; Chin, J.E.; Wunder, J.S.; Andrulis, I.L.; Gazdars, A.F.; Willman, B.; Griffith, Hoff D.D.; Roninson, I.B. Quantitative Analysis of MDR1 (Multidrug Resistance) Gene Expression in Human Tumors by Polymerase Chain Reaction. *Proceedings of the National Academy of Sciences*. **1990**, 87(18), 7160-7164.
- Pack, D.W.; Putnam, D.; Langer, R. Design of Imidazole-Containing Endosomolytic Biopolymers for Gene Delivery. *Biotechnology and Bioengineering*. **2000**, 67(2), 217-223.
- Pranoto, Y.; Rakshit, S.K.; Salokhe, V.M. Enhancing Antimicrobial Activity of Chitosan Films by Incorporating Garlic Oil, Potassium Sorbate and Nisin. *LWT-Food Science and Technology*. **2005**, 38(8), 859-865.
- Sanford, M. S. Role of Organelle pH in Tumor Cell Biology and Drug Resistance. *Drug Discovery Today*. **1999**, 4(1), 32-38.
- Scheeren, E.L.; Nogueira, D.R.; Macedo, L.B.; Vinardell, M.P.; Mitjans, M.; Infante, M.R.; Rolim, C.M.B. PEGylated and Poloxamer-Modified Chitosan Nanoparticles Incorporating a Lysine-Based Surfactant for pH-Triggered Doxorubicin Release. *Colloids and Surfaces B: Biointerfaces*. **2016**, 138, 117-127.
- Sehgal, D.; Vijay, I. K. A Method for the High Efficiency of Water-Soluble Carbodiimide-Mediated Amidation. *Analytical Biochemistry*. **1994**, 218, 87-91.

- Shi, C.; Zhu, Y.; Ran, X.; Wang, M.; Su, Y.; Cheng, T. Therapeutic Potential of Chitosan and its Derivatives in Regenerative Medicine. *Journal of Surgical Research*. **2006**, 133(2), 185-192.
- Shen, Y.; Tang, H.; Zhan, Y.; Kirk, E.A.V.; Murdoch, W.J. Degradable Poly(β -Amino Ester) Nanoparticles for Cancer Cytoplasmic Drug Delivery. *Nanomedicine: Nanotechnology, Biology and Medicine*. **2009**, 5(2), 192-201.
- Simon, S.M.; Schindlert, M. Cell Biological Mechanisms of Multidrug Resistance in Tumors. *Proceedings of the National Academy of Sciences*. **1994**, 91(9), 3497-3504.
- Song, H.; Zhang, J.; Wang, W.; Huanh, P.; Zhang, Y.; Liu, J.; Li, C.; Kong, D. Acid-Responsive PEGylated Doxorubicin Prodrug Nanoparticles for Neuropilin-1 Receptor-Mediated Targeted Drug Delivery. *Colloids and Surfaces B: Biointerfaces*. **2015**, 136, 365-374.
- Special Surgical Techniques.
<http://www.cancer.org/treatment/treatmentsandsideeffects/treatmenttypes/surgery/special-surgical-techniques> (accessed April 20, 2016).
- Tabin, C.; Bradley, S.M; Bargmann, C.I.; Weinberg, R.A.; Papageorge, A.G.; Scolnick, E.M.; Dhar, R.; Lowv, D.R.; Chang, E.H. Mechanism of Activation of a Human Oncogene. *Nature*. **1982**, 300(5888), 143-149.
- Takeichi, M. Cadherin Cell Adhesion Receptors as Morphogenetic Regulator. *Science*. **1991**, 251(5000), 1451-1455.
- Tian, T.; Bae, Y.H. Cancer Nanomedicines Targeting Tumor Extracellular pH. *Colloids and Surfaces B Biointerfaces*. **2012**, 99, 116-126.
- Tiwari, G.; Tiwari, R.; Sriwastawa, B.; Bhari, L.; Pandey, P.; Bannerjee S.K. Drug Delivery Systems: An Updated Review. *International Journal of Pharmaceutical Investigation*. **2012**, 2(1), 2-11.
- Tong, R.; Cheng J. Anticancer Polymeric Nanomedicines. *Polymer Reviews*. **2007**, 47, 345-381.

- Torchilin, V. P. Block Copolymer Micelles as a Solution for Drug Delivery Problems. *Expert Opinion on Therapeutic Patents*. **2005**, 15(1), 63–75.
- Tu, X.; Wang, L.; Cao, Y.; Ma, Y.; Shen, H.; Zhang, M.; Zhang, Z. Efficient Cancer Ablation by Combined Photothermal and Enhanced Chemo-Therapy Based on Carbon Nanoparticles/Doxorubicin@SiO₂ Nanocomposites. *Carbon*. **2016**, 97, 35-44.
- UNSCEAR. *Sources and Effects of Ionizing Radiation*; United Nations Scientific Committee on the Effects of Atomic Radiation Report to the General Assembly, United Nations: New York, 1993.
- UNSCEAR. *Sources and Effects of Ionizing Radiation*; 2; United Nations Scientific Committee on the Effects of Atomic Radiation Report to the General Assembly, United Nations: New York, 2000.
- Upton, A.C.; Albert, R.E.; Burns, F.J.; Shore R.E. Historical Perspectives on Radiation Carcinogenesis. *Radiation Carcinogenesis*. **1986**, Elsevier, New York, 1-10.
- Vasey, P.A.; Kaye, S.B.; Morrison, R.; Twelves, C.; Wilson, P.; Duncan, R.; Thomson, A.H.; Murray, L.S.; Hilditch, T.E.; Murray, T.; Burtles, S.; Fraier, D.; Frigerio, E.; Cassidy, J. Phase I Clinical and Pharmacokinetic Study of PK1 [N-(2-Hydroxypropyl)methacrylamide Copolymer Doxorubicin]: First Member of a New Class of Chemotherapeutic Agents—Drug-Polymer Conjugates. *Clinical Cancer Research*. **1999**, 5(1), 83-94.
- Vejpongsa, P.; Edward, T.H. Prevention of Anthracycline-Induced Cardiotoxicity. *Journal of the American College of Cardiology*. **2014**, 64(9), 938-945.
- Veronese, F.M.; Schiavon, O.; Pasut, G.; Mendichi, R.; Andersson, L.; Tsirk, A.; Ford, J.; Wu, G.; Kneller, S.; Davies, J.; Duncan, R. PEG-Doxorubicin Conjugates: Influence of Polymer Structure on Drug Release, in Vitro Cytotoxicity, Biodistribution, and Antitumor Activity. *Bioconjugate Chemistry*. **2005**, 16(4), 775-784.
- Veronese, F.M.; Harris, J. M. Introduction and Overview of Peptide and Protein PEGylation. *Advanced Drug Delivery Reviews*. **2002**, 54(4), 353-356.

- Veronese, F.M.; Schiavon, O.; Pasut, G.; Mendichi, R.; Andersson, L.; Tsirk, A.; Ford, J.; Wu, G.; Kneller, S.; Davies, J.; Duncan, R. PEG-Doxorubicin Conjugates: Influence of Polymer Structure on Drug Release, in Vitro Cytotoxicity, Biodistribution and Antitumor Activity. *Bioconjugate Chemistry*. **2005**, 16(4), 775-784.
- Wang, D.; Li, L.; Zhang, P. Synthesis of Some Neutral, Water-Soluble Carbodiimides and Their Use in the Formation of Peptide Bonds. *Scientia Sinica Series B*. **1987**, 30, 449-459.
- Wieder, K. J.; Palczuk, N. C.; Es, T.; Davis, F. F. Some Properties of Polyethylene Glycol: Phenylalanine Ammonia-Lyase Adducts. *Journal of Biological Chemistry*. **1979**, 254(24), 12579–12587.
- Zhang L.; Zhang P.; Zhao Q.; Zhang Y.; Cao L.; Luan Y. Doxorubicin-Loaded Polypeptide Nanorods Based on Electrostatic Interactions for Cancer Therapy. *Journal of Colloid and Interface Science*. **2016**, 464, 126-136.
- Zhou, L.; Cheng, R.; Tao, H.; Ma, S.; Guo, W.; Meng, F.; Liu, H.; Liu, Z.; Zhong, Z. Endosomal pH-Activatable Poly(Ethylene Oxide)-graft-Doxorubicin Prodrugs: Synthesis, Drug Release and Biodistribution in Tumor-Bearing Mice. *American Chemical Society, Biomacromolecules*. **2011**, 12(5), 1460-1467.

APPENDIX A

SUPPLEMENTARY FIGURES AND CALCULATIONS

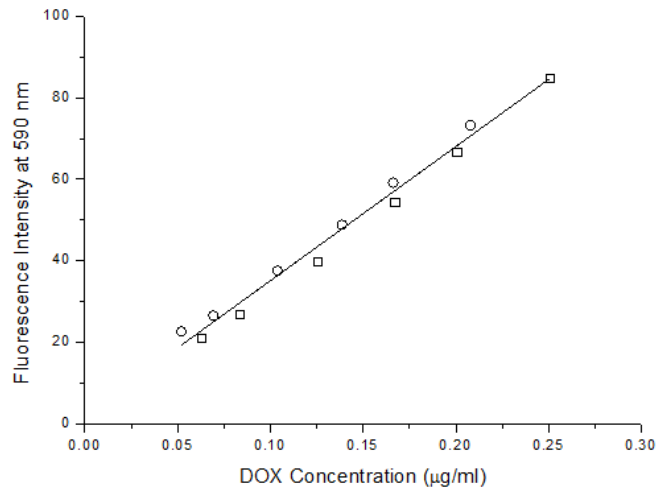


Figure A.1. DOX Calibration Curve using Fluorescence Intensity at 590 nm (Prepared in PBS Buffer)

Excitation Wavelength:480 nm, Slit Width: Excitation 5 nm, Emission 20 nm (Equation= $0.003 \times I - 0.005$)

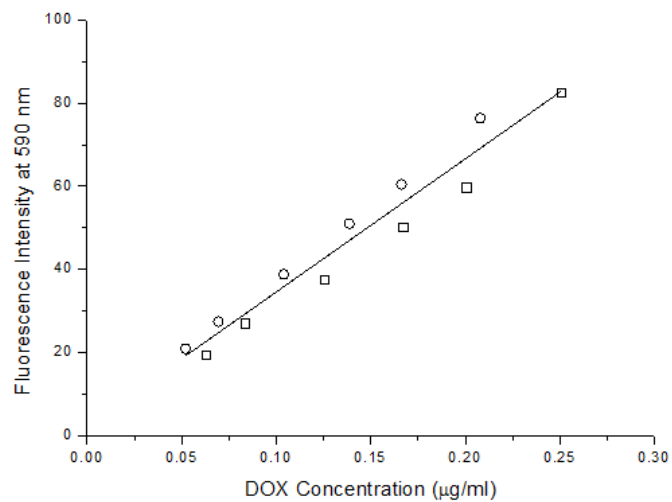


Figure A.2. DOX Calibration Curve using Fluorescence Intensity at 590 nm (Prepared in Acetate Buffer)

Excitation Wavelength:480 nm, Slit Width: Excitation 5 nm, Emission 20 nm (Equation= $0.00297 \times I - 0.001$)

- Sample Calculation of Drug Release (for mPEG-HYD1-DOX in PBS at 72h)

The following data given below was used for calculations:

amount of mPEG-HYD1 used (mg)	1.58
M_{DOX} (g/mol)	542
$M_{conjugate}$ (g/mol)	~ 5600
volume of dialysis media (mL)	25
DOX functionality of mPEG-HYD1-DOX	0.62

About 1.50 mg conjugate was weighted for each dialysis experiment. DOX functionality of the conjugates was determined previously.

Intensity at 590 nm (excitation wavelength=480 nm, excitation slit width=5nm, emission slit width= 20 nm and scan rate= 125nm/min.) was measured and given below:

time (h)	intensity	dilution factor	intensity (after dilution)
72	114.12	2	62.2

Since the intensity did not fit in the range of calibration curve, the sample was diluted 2 times and that value was also recorded.

Amount of DOX released was calculated as below in which 2 was corresponding to the dilution factor and 25mL was the dialysis volume.

$$\text{Amount of DOX released (Ct)} = (0.003 * 62.2 - 0.005) * 2 * 25 = 9.1 \text{ mmol}$$

$$\text{Amount of DOX in the conjugate initially (Ci)} = \frac{1.58 * 580 * 0.62 * 1000}{5600} = 101.5 \text{ mmol}$$

$$\text{DOX release \%} = \frac{9.1}{101.5} * 100\% = 8.95 \%$$

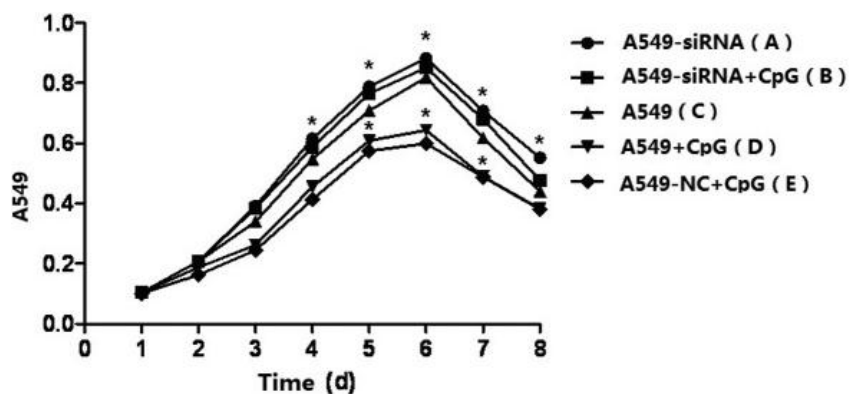
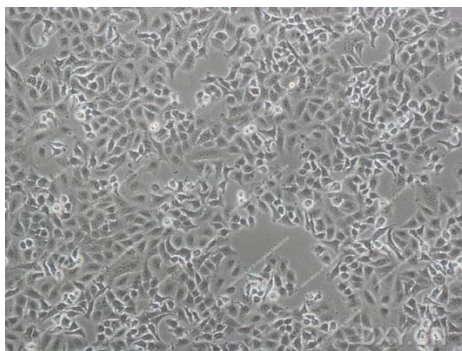


Figure A.3. Morphology and Growth Curve of A-549 Cell Line (Source: Barnie et al., 2014).

Table A.1. Final Concentrations of Samples in the Well for MTT Test

Concentration of free DOX ($\mu\text{g/ml}$)	Concentration of DOX-conjugated DDS ($\mu\text{g/ml}$)
100	1500
50	750
25	375
10	150
5	75
2.5	37.5
1.0	15
0.5	7.5
0.25	3.5
0.1	1.5
0.05	0.75

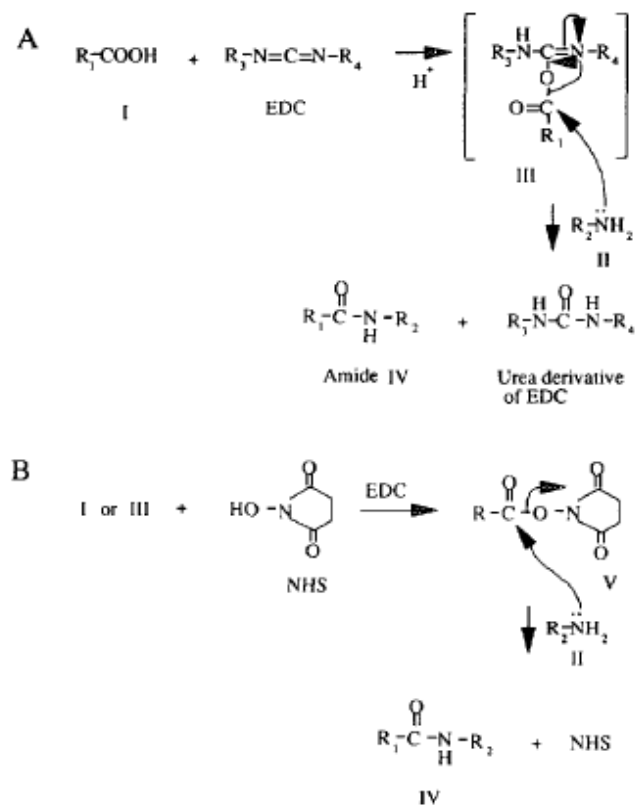


Figure A.4. Amide Formation Reactions Using EDC and NHS
(Source: Conde et al., 2014).

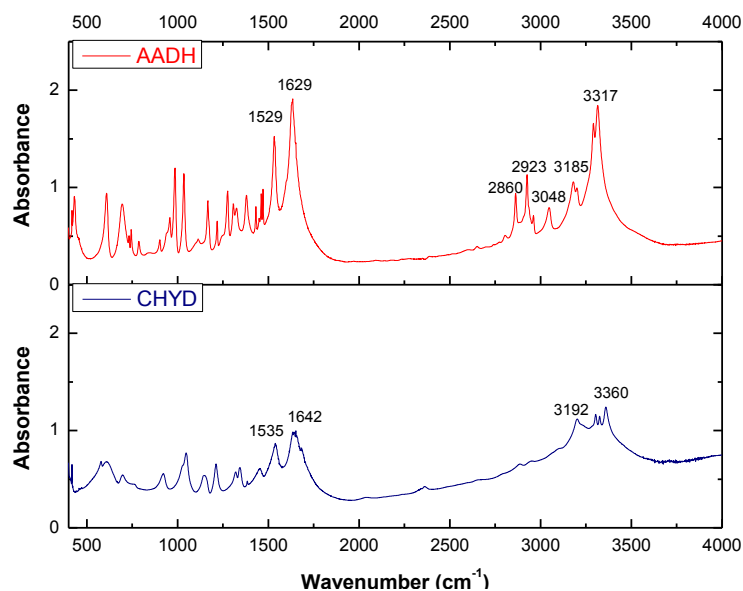
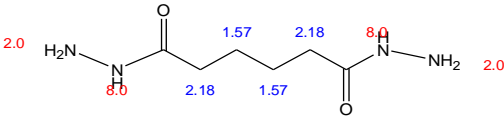
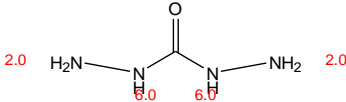
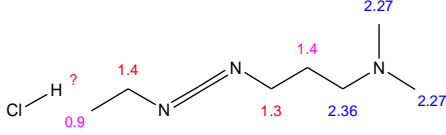
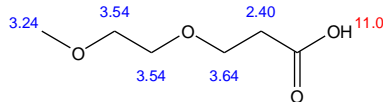
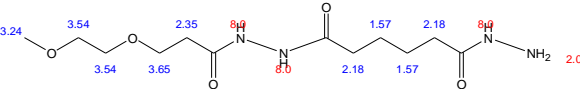
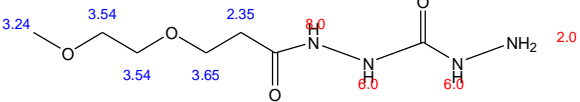


Figure A.5. FTIR Spectra of Adipic Acid Dihydrazone and Carbohydrazide

Table A.2. ¹H NMR Chemical Shift Estimations

Abbreviation	Molecule	Chemical Structure and Theoretical ¹ H NMR Chemical Shifts
AADH	Adipic acid dihydrazide	
CHYD	Carbohydrazide	
EDC	N-(3-Dimethylamino propyl)-N'-ethylcarbodiimide hydrochloride	
mPEG-COOH	Methoxy polyethylene glycol propionic acid	
mPEG-HYD1	Methoxy polyethylene glycol adipic acid hydrazide	
mPEG-HYD2	Methoxy polyethylene glycol adipic acid hydrazide	

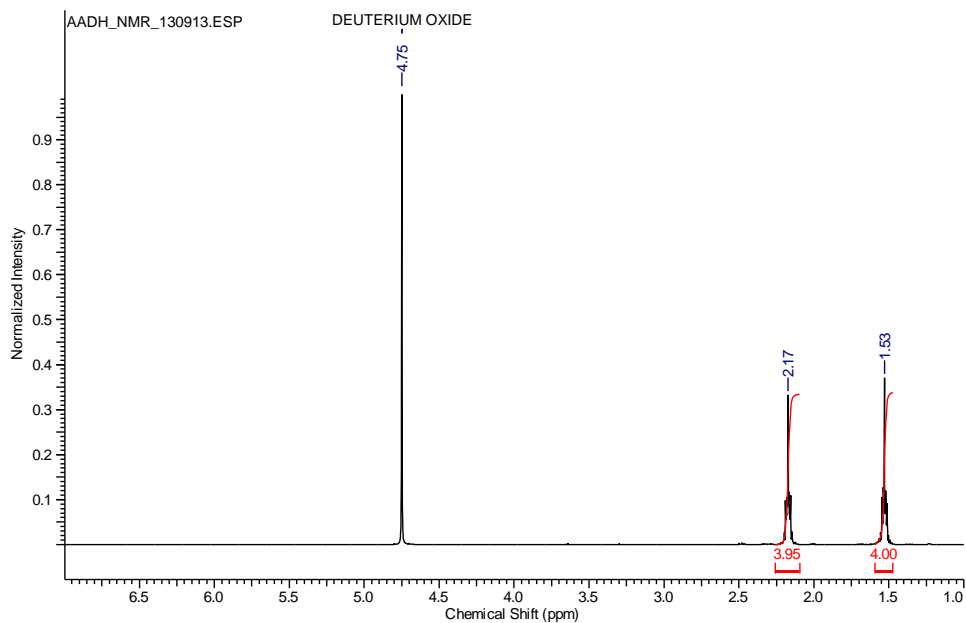


Figure A.6. NMR Spectrum of AADH in D₂O

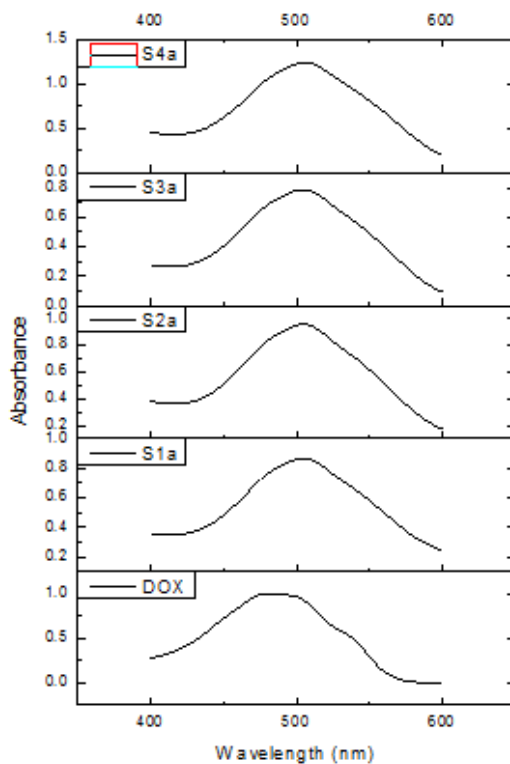


Figure A.7. UV-Vis Spectroscopy Result for Determination of Functionality

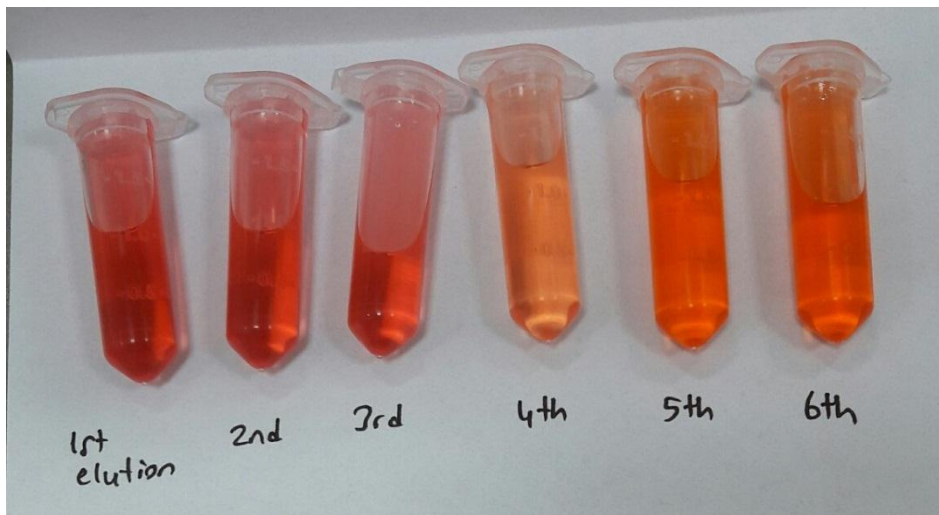


Figure A.8. Fractions Obtained from Columns (10 mL Bed Volume) Containing Sephadex-LH20 Resin.

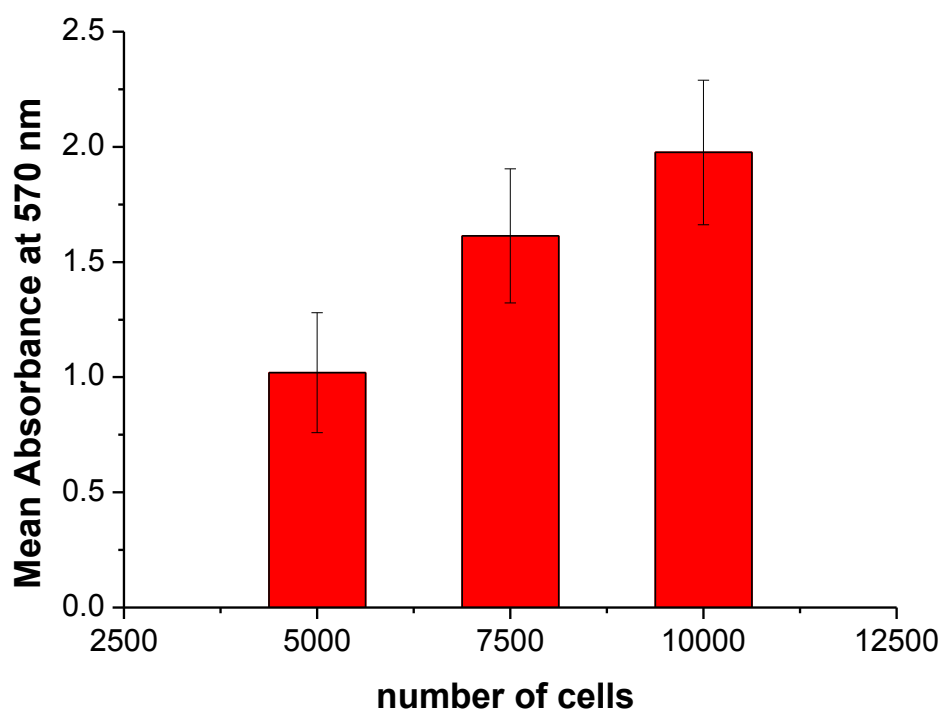


Figure A.9. Absorbance Values of A549 Cell Lines as a Function of Number of Cells Used in MTT Assay